DEVELOPMENT OF A FAST AND SIMPLIFIED MODEL OF HVDC CONVERTER IN PSCAD AND PERFORMANCE COMPARISON WITH LCC CONFIGURATIONS

By

Parisa Khodaei

A thesis to be submitted to the Faculty of Graduate Studies of

The University of Manitoba

in partial fulfillment of the requirements for the degree of

Master of Science

Department of Electrical and Computer Engineering

University of Manitoba

Winnipeg, Manitoba, Canada

ABSTRACT

HVdc systems are facing increasing complications in simulation because of the need to combine various types of converters to achieve better performance results. In practice, most of the HVdc systems operate by utilizing line-commutated converters (LCCs). The LCCs use thyristors as switching devices to convert alternating currents (ac) to dc and vice versa. There are advantages and disadvantages associated with the employment of LCCs in HVdc transmission systems. One aspect of challenges related to LCC-based HVdc systems is their simulation run time, as the switching functionality of LCC components causes considerable delay in the simulation run time. For complex simulation cases, decent hardware (in terms of CPU and GPU) is required to run successfully even though they will still be time-consuming.

In this research, a new simplified and fast model of converters has been designed and developed in PSCAD/EMTDC. The new component is built upon steady-state equations governing the LCCs without taking the detailed switching behavior into account. The new component relies on the measurement of the dc current using the existing multimeter in PSCAD. A dc voltage source is customized for the dc side of the converter, while the ac side is modelled as an ac current injected source. The new model can be utilized in place of the LCCs (either on inverter or rectifier sides of HVdc transmission systems for screening studies. The simulation results show that the new component reduces the simulation run time compared to the equivalent LCC-based model without significant accuracy loss. The new component could also handle commutation failures. The application of the new component could be highlighted in complicated HVdc models when there is a need for multiple runs to tune the system's control parameters.

ACKNOWLEDGEMENT

I would like to express my deepest gratitude to my advisor, Professor Aniruddha Gole, whose vision and support opened a new direction in my academic journey. His guidance throughout my graduate studies facilitated the successful completion of this research.

I sincerely thank the members of my examining committee, Dr. Udaya Annakkage and Dr. Jenny Zhou, for their time, valuable feedback, and constructive comments.

My heartfelt appreciation goes to my husband, Dr. Ali Maddahi, for his unwavering support. This achievement would not have been possible without his encouragement.

I am deeply thankful to my parents for their constant support, which have always been with me.

Finally, I am grateful to my colleagues in the Power Systems Simulation Laboratory for their support and collaboration—special thanks to Dr. Kustav Dey, Narges Zarean Shahraki, Dr. Ajinkya Sinkar and Shrimal Koruwage.

TABLE OF CONTENTS

LIST OF FIGURES

LIST OF ACRONYMS

HVdc	High voltage direct current
LCC	Line-commutated converter
ac	Alternating current
dc	Direct current
VSC	Voltage source converter
MMC	Modular multilevel converter
EMTP	Electromagnetic transients program
FACTS	Flexible ac transmission systems
PSCAD	Power systems computer aided design
EMTDC	Electromagnetic Transients including dc
IGBT	Insulated gate bipolar transistor
SCR	Short circuit ratio
CCC	Capacitor commutated converter
STATCOM	Static synchronous compensator
GTO	Gate-turnoff thyristor
LV	Low voltage
HV	High voltage
FB	Full bridge
VDCOL	Voltage dependent current order limiter
CEC	Current error control
PI	Proportional-integral
FS	Fast and simplified
AOR	Alpha-order rectifier
AOI	Alpha-order inverter

LIST OF NOMENCLATURE

V_l	Rated line voltage
Z_t	Thevenin impedance
P_d	dc power
L_c	Inductance
L_d	Smoothing reactance
v_a	Phase-a ac voltage
v_b	Phase-b ac voltage
v_c	Phase-c ac voltage
V_m	Line-to-neutral ac voltage peak value
ω	Network frequency
v_{ac}	Line-to-line voltage between phase-a and phase-c
v_{ba}	Line-to-line voltage between phase-b and phase-a
v_{cb}	Line-to-line voltage between phase-c and phase-b
t	Time
α	Firing angle / Delay angle
μ	Conduction angle / Overlap angle
V_{do}	Ideal no-load direct voltage
V_{LN}	RMS line-to-neutral voltage
V_{LL}	RMS line-to-line voltage
V_d	dc voltage

I_d	dc current
I_{L1}	RMS value of fundamental frequency component of ac line-to-neutral current
$\cos\phi$	Power factor / Displacement factor
X_c	Transformer's leakage reactance
Q	Reactive power
γ	Extinction angle

CHAPTER I

1. INTRODUCTION

High voltage direct current (HVdc) systems employ direct current (dc) to transmit electric power for long distances. Nowadays, HVdc systems are facing increasing complications in simulation because of the need for combining various types of converters to achieve better performance results aiming to address increasing demands for power in industries; therefore, the modeling of such systems is becoming a challenge.

In practice, most of the HVdc systems operate by utilizing line-commutated converters (LCCs). The LCCs use thyristors as switching devices to convert alternating currents (ac) to dc and vice versa. There are advantages and disadvantages associated with the employment of LCCs in HVdc transmission systems. One aspect of challenges related to LCC-based HVdc systems can be their simulation studies.

1.1. Motivation

LCCs are widely used in inverter and rectifier sides of HVdc systems. They feature many practical advantages which have made them one of the top technologies used in the development of HVdc systems. Despite their drawbacks, they are still used in hybrid configurations with other types of converters such as voltage source converters (VSCs) and modular multilevel converters (MMCs). From the simulation studies perspective, there still exists room for improvement such as designing equivalent models of LCCs to reduce the simulation times, specifically, during the controller parameter tuning process [1].

1.2. Problem Definition

It is important to ensure the proper performance of large power networks before or during the installation processes. One of the main parts of long-distance transmission systems is the converter settings. Converters refer to both rectifiers and inverters which are responsible for converting ac to dc and dc to ac, respectively. To avoid extra installation or repair costs in practical projects, it is necessary to simulate and analyze various aspects of HVdc transmission systems in advance.

In terms of the converters, LCCs are extensively employed at every end of transmission lines as they can transmit more power compared to VSC configurations while having less expensive installation costs. Despite the advantages of LCCs in HVdc systems, they are prone to commutation failure because of the influence of the ac system [2]. In practical applications, the LCCs are still of interest as they are cost-effective compared to VSCs and MMCs.

From the simulation studies' point of view, the LCCs make the entire simulation cases slow [2] because they are represented in the context of a set of detailed valve group models where many

switching devices are used to emulate a close-to-real model of LCCs. This causes a long simulation time when multiple LCCs are used in rectifier and/or inverter sides of single or multi-terminal networks. The more the number of LCCs is, the slower the simulation time would be. This drawback will be highlighted more when there is a need for tunning the controller parameters, in a complicated case study, which requires several runs. Therefore, one of the main problems associated with LCCs in simulation studies is long time of simulation runs.

Although optimization-based simulation studies provide accurate controller parameter values in the tuning process, they are still time-consuming and expensive in terms of hardware requirements. Depending on the number of variables to be tuned, a case study may need to be relegated to overnight or over the weekend computations [3]. This is evident specifically when the simulation case is complicated and includes a combination of LCC and VSC topologies or LCC-MMC ones. The cases can even be more complicated when there exist multi terminals in the network, each containing one or more LCC system. Such complex simulation cases will require decent hardware (in terms of CPU and GPU) to run successfully even though they will still be time-consuming.

1.3. Proposed Solution

Electromagnetic Transients Simulation programs (*i.e.*, emtp-type programs) are useful tools for the analysis of transient behaviors in large power networks. They allow for a precise representation of the power network [4], which is far more detailed as compared to representations used in load flow and stability programs. If the power network contains Flexible ac Transmission Systems (FACTS) or other power electronic apparatus, the emtp-type program can model the operation of

individual semiconductor switches and is also able to represent the controls in detail [5]. One of the well-known emtp-type simulation programs is PSCAD/EMTDC which features the ability to automatically perform multiple simulations on the same case while changing one or more variables at each run. For example, in non-linear models such as dc transmission lines, it is possible to control system gains, and time constants can be sequentially or randomly selected to find an optimum response to a disturbance [3].

In this research, a new simplified and fast model is proposed, in PSCAD/EMTDC, to replace LCCs in either inverter or rectifier sides of HVdc transmission systems. The new model can be used in lieu of LCCs in various configurations such as purely LCC, LCC-VSC, and LCC-MMC in both rectifier and inverter sides of single or multi-terminal HVdc systems. The new component is built upon the employment of steady-state equations governing the LCCs while removing harmonics from the simulation results and overcoming the issue of the long simulation time in simulation studies. This is useful in the controller parameter tuning of slow dynamic studies. This thesis will also investigate whether the developed model works for faults and other transient studies.

1.4. Thesis Objectives

This thesis aims to develop a new component as a replacement for LCCs, in PSCAD/EMTDC, for screening studies, while maintaining the accuracy of the overall dynamic response. The new model is simpler and faster as it uses the steady-state converter equations; however, it does ignore the detailed switching behavior of the converter. The main objectives of the thesis are:

(i) to test the validity of the new component when being used along with the conventional LCC modules in HVdc models as well as in the presence of commutation failure;

(ii) to examine the steady state behavior of the new component when it replaces LCCs on both rectifier and inverter sides; and,

(iii) to reduce the simulation time by replacing the entire LCC component with the newly developed model in PSCAD/EMTDC program.

1.5. Thesis Structure

Chapter II presents a literature review on the history of HVdc transmission systems followed by various configurations of HVdc systems and control strategies used for LCCs. In Chapter II, the current solutions of the control parameter tuning process are briefly explained as well. Chapter III describes the theory and mathematical modeling behind the LCC configurations in detail along with providing the governing equations used for the development of a new component in PSCAD/EMTDC. In Chapter IV, the implementation procedure is explained followed by representing the simulation results and discussion. Chapter V outlines the contributions of this thesis and the suggested future work.

CHAPTER II

2. RELEVANT BACKGROUND

A high voltage direct current (HVdc) electric power transmission system uses direct current (dc) for the bulk transmission of electrical power, in contrast with the more common alternating current (ac) systems [6]. Although ac transmission has been used as a preferred means for electric power transport globally over the past century, its certain limitations such as shorter distance constraints, transmission capacity, and the impossibility of connecting two ac power networks of different frequencies have drawn attention to the use of HVdc systems [7]. Using HVdc transmission, it is possible to transmit power between two ac networks of different frequencies and non-synchronized. This is how the power flow is still controllable through the HVdc line in an independent manner.

The basic idea behind the development of HVdc systems is to transmit a certain power with high voltage and use of direct current to reduce power loss. The greater the current, the larger the amount of power loss will be. However, for a certain amount of power to be transmitted, if the

voltage is doubled, the current level will be halved, resulting in a reduction in power loss (in the form of heat) by a factor of four [6].

Since the 1930s, there has been interest in designing and developing high-voltage transmission lines due to the limitations of AC transmission systems and the power loss that occurs over long distances at low voltages [8].

2.1. Evolution of HVdc Transmission Systems

The very first version of HVdc systems used mercury-arc valves to convert alternating currents into dc [9]. A mercury-arc valve contains a type of cold cathode gas-filled tube but is unique in that the cathode is made from a pool of liquid mercury, which allows for self-restoration [10]. However, despite the successful operation of the mercury-arc schemes, the incidence of arc backs, considerable maintenance, and voltage limitations led to the development of solid-state technology, initially using thyristors, and later using gate turn-off devices such as insulated gate bipolar transistors (IGBT) [11].

The thyristor technology had a significant impact, not only because the valve cost was initially comparable to the cost of the mercury-arc valve, but also due to the overall economic effect on the station plant and layout [11]. Even before the commissioning of the last two mercury-arc schemes (Nelson River and Kingsnorth), the small experience gained with thyristor valves was sufficient to discourage any further development of the mercury-arc technology [11].

The technical reasons supporting the use of solid-state HVdc transmission are essentially the same as those given for the mercury-arc schemes. However, a brief look at the solid-state schemes will help us understand the great progress made with the new technology. The development of

thyristor valves for HVdc began in the late 1960s. The first complete HVdc scheme based on thyristor, in Canada, was the Eel River scheme, which was built by General Electric Company and went into service in 1972 [6] and [11]. The Eel River converter station, first, consisted of two separate 12-pulse bidirectional solid-state non-synchronous HVdc ties of 4800 thyristors, each nominally rated 160 MW, connecting 230 kV transmission systems of Hydro-Québec and New Brunswick Power [12].

Solid-state HVdc transmission systems are available in various topologies, with the traditional systems using thyristor devices. The thyristor can be turned on by supplying its gate with a turn on-pulse, but to turn off, the ac line-line voltage must provide the reverse bias [13]. Hence, the HVdc converter is referred to as a line-commutated converter (LCC). The term "line commutated" refers to the conversion process that relies on the ac voltage in the successful transfer (*i.e.*, "commutation" of the current from one switch to next one in conduction sequence). LCC-HVdc systems are well-suited for long-distance and large-capacity power transmission. If the ac voltages fluctuate with loading or after transients, there is a danger that the thyristor valve does not turn off at the appropriate time, resulting in a "commutation failure".

Figure 2.1 shows the schematic diagram of the 6-pulse Graetz bridge, which is the building block of the LCC-HVdc transmission system. Each bridge consists of 6 thyristors which are considered as uncontrolled semiconductor devices. The thyristors turn on by a firing pulse with a delay, called a firing angle or alpha, and turn off based on the commutation process from one switching device to another one [6].

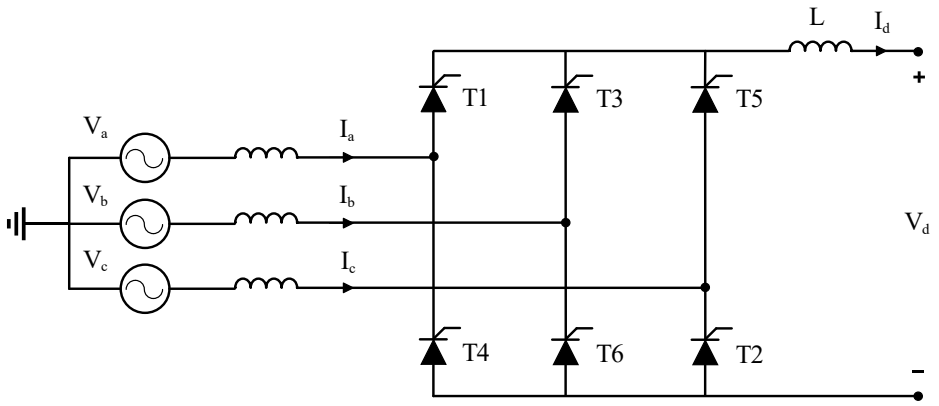

Figure 2.1 Schematic diagram of 6-pulse Graetz bridge [14]

2.2. HVdc Transmission Technologies

2.2.1. Line commutated Converters (LCCs)

LCC is the first and still widely used technology in HVdc systems. Transmission systems using conventional thyristor-based LCC-HVdc converters offer many advantages over ac transmission systems namely:

(i) They carry more power over a given right of way,

(ii) They can connect non-synchronous ac systems,

(iii) Transmission power losses on long lines are low due to the entire cross section of the conductor being available for conduction.

(iv) They are suitable for underground and underwater power transmission using cables [15] and [16], because the cable capacitance is an open circuit to the dc voltage.

However, LCCs use the system ac voltage for thyristor turnoff, which means that a reactive power source is required to support this ac voltage. Additionally, LCCs require a significant amount of space to accommodate ac filters and reactive power compensation equipment [15]. They are

difficult to operate when the connected ac networks are weak, *i.e.*, having a high Thevenin impedance, which makes it difficult to regulate the ac voltage. The system strength is measured in terms of a "short circuit" ratio (SCR), which is loosely defined as the ratio of short circuit level to the converter's rated power. For a circuit shown in Figure 2.2, the SCR can be calculated as follows [17]:

$$SCR = \frac{SCMVA}{P_d} = \frac{V_l^2/Z_t}{P_d} \tag{2.1}$$

where P_d denotes the dc power and V_l is the rated line voltage. Also, Z_t is the Thevenin impedance which is normally close to being purely inductive (*i.e.*, $\angle Z_t = 90°$), therefore, the SCR is a scalar number. Occasionally, one may define the SCR to be, for example, $2.5\angle 80°$, meaning that the SCR magnitude is 2.5 and the Thevenin impedance angle is 80°.

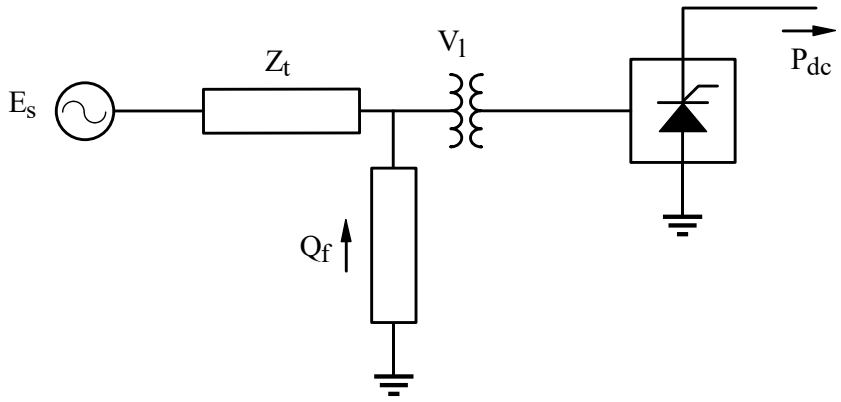

Figure 2.2 Overall schematic of a converter connected to an ac system.

A certain minimum SCR level must be maintained at the location where the converter is to be installed [18]. A system where the SCR is below about 2.0 can be expected to result in problems such as excessive load rejection over-voltages and susceptibility to commutation failures. To

overcome these disadvantages, several solutions have been proposed, such as the use of capacitor commutated converters (CCCs) [16], voltage sourced converters [19] or a solid-state static synchronous compensator (STATCOM) in conjunction with a series compensated LCC to overcome the issues raised by thyristor-based LCC-HVdc converters [20].

The LCC also has the disadvantage of occupying large areas such that dc landing points are dense and ac faults may lead to multi-circuit dc commutation failures, which will have a serious adverse impact on the stability of the receiving end system. At the same time, economically developed areas do not have the conditions for large-scale construction of LCC due to land resource constraints [21]. In addition, LCC-HVdc systems adopt semi-controlled commutation device, which, however, are prone to the commutation failure because of the influence of the ac system [2].

2.2.2. Voltage Sourced Converter Based HVdc

As an alternative to LCCs, an HVdc system can be also implemented with voltage source converters (VSCs) [22]. VSCs use gate-turnoff devices such as Gate-turnoff thyristors (GTOs) or, more recently, insulated gate bipolar transistors (IGBT). These devices can be ordered to turn on with a gate pulse in the same manner as the thyristor, but they can be turned off with an “off” gate pulse. Hence, they do not rely on the ac voltage for successful commutation. Although the LCC-HVdc system can handle higher power and voltage ratings than those of the insulated gate bipolar transistors (IGBT)-based VSC-HVdc system, the VSC overcomes the chief disadvantages of LCCs such as the reduction of harmonic distortion on both the ac and dc sides. Thus, the size of output

filters can be reduced using VSC-HVdc systems [22]. VSCs are also not prone to commutation failures because they do not rely on the ac voltage for commutation.

VSCs started to appear in HVdc in 1997 with the experimental Hellsjön–Grängesberg project in Sweden. By the end of 2011, this technology had captured a significant proportion of the HVdc market [23]. The development of higher-rated IGBTs, gate turn-off thyristors (GTOs), and integrated gate-commutated thyristors (IGCTs) in VSC-HVdc technology, have spurred the implementation of this technology. Indeed, VSCs can even be operated at unity or even leading power factor, and their rapid controllability permits them to be used in a voltage support role in addition to their primary purpose of power transmission [24]. Manufacturers such as Hitachi-ABB, Siemens, and GE have extended the use of HVdc down to blocks as small as a few tens of megawatts and overhead lines as short as a few dozen kilometers. There are several variants of VSC technology; most installations built until 2012 use pulse-width modulation (PWM) in a circuit that is effectively an ultrahigh-voltage motor drive [23]. The disadvantages associated with these converters are their excessive cost and losses and their relatively smaller ratings compared to the conventional thyristor based LCCs [24] - [25].

A converter-hybrid HVdc system uses converters that are formed with LCC and VSC. Most of the research studies focus on the series converter-hybrid HVdc system with LCC and VSC connected in series [24], [26] [27]- [28]. For example, Qahraman and Gole [24] proposed a series hybrid converter topology that comprises of one VSC and one LCC converter. Such a topology had already been used in certain active filter arrangements; however, its application to the power transmission was novel [26]. In this hybrid arrangement, the conventional converter, which has relatively low conversion loss, handles the bulk of the power transmission, whereas the

incremental power is transferred using the VSC converter, providing a control flexibility and the voltage support for the conventional converter [24].

Among the VSCs, the modular multilevel converter (MMC) is a highly regarded topology. The MMC has several features such as modular construction, high reliability, and cost-effectiveness because it uses the low-voltage insulated gate bipolar transistor (LV-IGBT) technology to reach high-voltage (HV) operation. The MMC is directly connected to medium-voltage (MV) and high-voltage (HV) grids without any step-up transformer. These features are potentially useful for a wide range of applications. Furthermore, it requires a high-performance control platform to process many gating signals [22]. In recent years, with the development of power electronic devices, MMC-HVdc systems have drawn much attention in academia for their advantages of (*i*) employing fully controlled devices, (*ii*) no commutation failure, (*iii*) independent control of the active and reactive power, (*iv*) low switching frequency, (*v*) no demand for ac filters and reactive compensation, and (*vi*) operation with passive or weak ac systems [29], [30] and [31]. However, the MMC-HVdc systems themselves have a higher cost and a lower transmission capacity compared to the LCC-HVdc [29] and [32].

The parallel operation of MMC-HVdc and LCC-HVdc realizes the complementarity of these two HVdc transmission topologies, which can not only supply power to the passive network or a weak ac system, but also make full use of LCC-HVdc's high-capacity transmission capacity and save costs [29]. Overall, the advantages and disadvantages of each of LCC and MMC-HVdc system have encouraged the researchers to combine them, aiming to achieve better performance by balancing the pros and cons of each topology [33]- [34]. In the hybrid LCC-MMC configuration, various topologies have been proposed, mostly on the inverter side. To integrate the advantages of LCC-HVdc and MMC-HVdc to the greatest extent, the hybrid HVdc system has

become an important development direction of the HVdc systems. For instance, Lv *et al.* [21] studied a hybrid system by considering LCC in series with MMCs on the inverter side. In this hybrid HVdc system topology, the dc voltage of the system will not drop to zero even if the LCC commutation fails, which is due to the existence of MMC on the inverter side. In such a topology, the hybrid HVdc system can transmit certain power to the ac network and reduce the impact of the ac network. At the same time, the LCC can prevent MMC fault current when HVdc transmission line fails. In the event of an HVdc line fault, the LCC and MMC on the inverter side can continue to operate unblocked [21].

The topology of such a hybrid HVdc system is illustrated in Figure 2.3. As shown, the rectifier side uses only LCC, and the inverter side employs the LCC in series with multiple MMCs. UR is the rectifier side ac system; UI(n+1) is the inverter side ac system connected by high-end converter LCCI on the inverter side. The low-end converter on the inverter side is composed of *n* MMCs in parallel, fed into the ac system in different areas through *n* converter transformers [21].

When LCC and MMC are connected in series at the receiving end, due to capacity limitations, multiple MMCs are typically required to be connected in parallel to match the capacity of the LCC [35]. Different from the centralized access to the ac system usually adopted by the LCC-HVdc system, the existence of LCC and parallel-connected MMCs enables the receiver to have decentralized access to the ac system. Considering the flexibility of the MMC control, the parallel-connected MMCs have a variety of potential control modes; however, the coordination of the control schemes and the influence of different connection modes on the system operation characteristics need to be further studied [35].

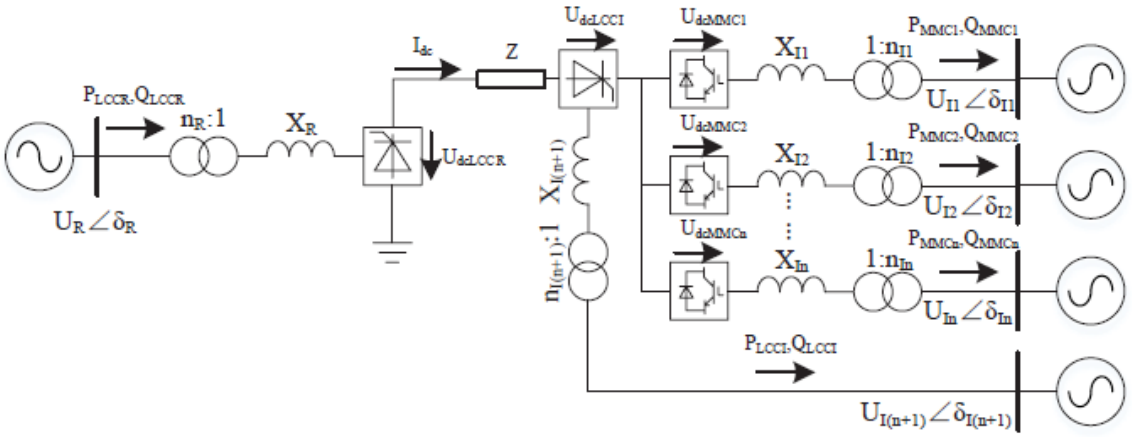

Figure 2.3 Hybrid configuration with LCC rectifier feeding multiple MMC receiving end inverters [21].

In a recent study, Xiao *et al*. [36] investigated the possibility of paralleling one LCC with one full bridge MMC (FB-MMC) on each terminal. In their proposed topology, the LCC and FB-MMC are connected in parallel so that they can share the same transmission line. The active-reactive power capability of the hybrid HVdc system is extended compared with the conventional LCC-HVdc system, and power reversal control without power interruption can be achieved by the coordination control of LCC and FB-MMC. Besides, this new hybrid HVdc system is capable of handling dc faults, as both LCC and FB-MMC have dc fault blocking capability. Moreover, they demonstrated that the power rating of FB-MMC can be designed to the low value while keeping the bulk-power transmission capability of LCC [36].

The FB-MMC is one of the highly effective solutions for HVdc systems, especially due to its capability of limiting the dc short-circuit current. Generally, the use of FB-MMC on a hybrid HVdc configuration with LCC is recommended for systems where there is no need for power reversion [37].

To summarize, the main advantages of a hybrid LCC-MMC HVdc system are [21] and [35]:

(i) It can transmit electricity to the occasions where land resources are scarce, or the ac system is weak.

(ii) It can still transmit a certain amount of active power even if the inverter LCC fails to commutate; this is because the MMCs can reduce the power shortage and improve the stability on the receiving-end system during the ac fault.

(iii) It can benefit from the multiple MMC parallel structure to maintain the stability of dc voltage, by allowing other MMC stations to participate in power regulation, in the event when one of the MMC stations fails out of operation.

(iv) It can limit the dc fault current passing through MMC by means of the single conductivity of LCC, *i.e.,* it has the ability of dc fault traversing.

(v) It can rely on the forced phase shift of the LCC to clear the dc fault without the need to configure expensive dc breakers or sub-modules with complex structures.

(vi) Due to the attractive characteristics of the MMC, the hybrid system requires less filter capacity and has stronger reactive voltage support capability.

2.3. Control strategies of LCC-based HVdc systems

Besides the advantages and disadvantages of various configurations of HVdc systems, the control strategies play important roles in achieving the design requirements. Since the focus of this research is on the LCC topology, the commonly used control strategies for the LCC are only explained here.

In general, the rectifier LCC adopts constant dc current control and minimum trigger angle control. Figure 2.4 shows the control block diagram of the LCC on the rectifier side of the HVdc

system. To prevent the LCC commutation failure due to the low voltage during the fault, voltage dependent current order limiter (VDCOL) control is added to the rectifier LCC [21].

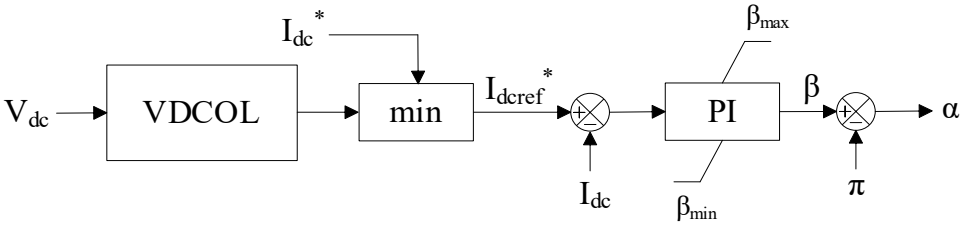

Figure 2.4 Control block diagram of LCC on rectifier side [21].

On the other side, the inverter LCC adopts constant extinction angle control and VDCOL control as backup control. The control block diagram of the inverter LCC is shown in Figure 2.5. To prevent the frequent switching between the constant extinction angle control and the VDCOL control, current error control (CEC) is added between the two controls. The current instruction value of the LCC on the inverter side should be 0.1 pu smaller than that of the LCC on the rectifier side to avoid the instability of the rectifier LCC and inverter LCC working under constant dc current control at the same time [21].

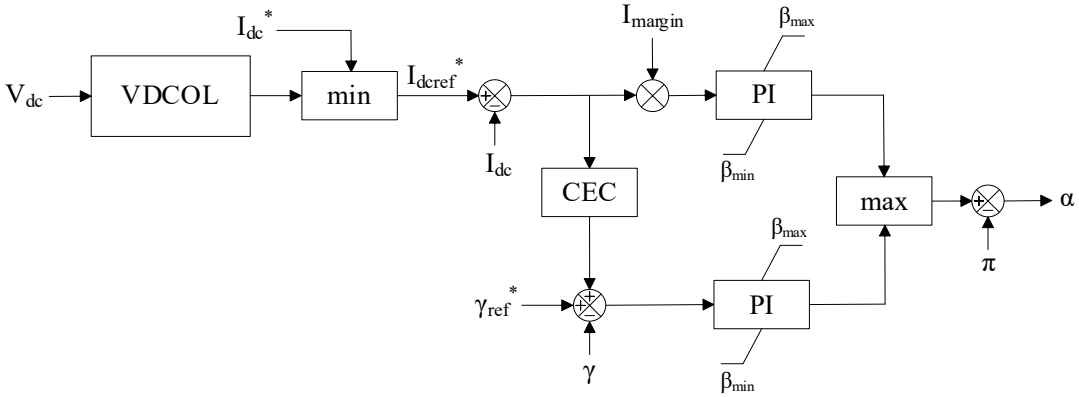

Figure 2.5 Control block diagram of LCC on inverter side [21].

The design and operation of LCC-HVdc schemes requires careful choice of controller parameters, including proportional-integral (PI) controller gains and VDCOL parameters. These parameters affect the dynamic behavior of HVdc schemes subjected to disturbances and set-point changes, as well as the in-service satisfactory performance of HVdc schemes. Two main approaches to tune these PI and VDCOL parameters are: (*i*) optimal control techniques using linearized state-space models; and (*ii*) manual tuning via trail-and-error to find feasible solutions. However, linearized models cannot explicitly model practical non-linear behaviors such as short-circuit faults, while manual tuning methods are time inefficient [38].

2.4. Essential Aspects Required for EMT Simulation Studies of HVdc Systems

In any HVdc system, tuning the controller parameters is one of the time-consuming tasks when using a digital simulation program. Usually, many simulation runs are required to obtain a desired system response. Most of the simulation cases containing LCC-HVdc systems are extremely slow because the valve group models are quite detailed.

Electromagnetic transient simulation programs (also known as emtp-type programs) are useful tools for the analysis of transient behaviors in large power networks. They allow for a precise representation of the power network [4], which is far more detailed as compared to representations used in load flow and stability programs. If the power network contains Flexible ac Transmission (FACTS) or other power electronic apparatus, the emtp-type program can model the operation of individual semiconductor switches and is also able to represent the controls in detail [5]. Similarly, transmission line, cable and machine models used in emtp-type programs are very accurate and valid to high frequencies. Emtp-type programs are thus useful in a range of applications such as

the determination of equipment stress, controller tuning of FACTS devices, and so on. The drawback associated with such programs is that they are relatively slow due to their heavy computational burden, and it takes a long time to complete the studies [5].

One of the well-known emtp-type simulation programs is PSCAD/EMTDC which features the ability to automatically perform multiple simulations on the same case while changing one or more variables at each run. For example, in non-linear models such as dc transmission lines, it is possible to control system gains, and time constants can be sequentially or randomly searched to find an optimum response to a disturbance. Similarly, if a transmission line is being switched, or a transformer is to be energized, a search for peak voltages can be undertaken by a varying point on wave switching. Depending on the number of variables sequenced, this feature can be time-consuming and may need to be relegated to overnight or over the weekend computations [3].

Optimization problems form an important category of power system studies that are often very hard or even impossible to solve using analytical techniques. To solve such problems, transient simulation programs usually host a ‘multiple run’ feature in which a series of runs is conducted, with the optimization parameters being successively varied over their corresponding feasible ranges to determine the best (or worst) case [3].

In terms of tuning HVdc controller parameter values, simulation-based optimization represents a viable alternative while considering large-signal disturbances and non-linearities. Simulation-based optimization allows simulation software - which can explicitly model large-scale non-linear behaviors - to be incorporated into a mathematical program to solve the optimization problem. This allows the modeling of transient behavior within conventional time-domain simulation programs (such as faults and switching events) to be considered within the optimization process. Simulation-based optimization represents a special type of optimization problem. The

optimization solver provides variable values to simulation software, which then runs a simulation with parameters initialized with those values [38]. The simulation output is then assessed using a merit function to return a value back to the optimization solver, where this value represents the objective function value. The solver uses the objective function value to infer a new set of variable values to test. This process is repeated until solver convergence conditions are met. Note that the term "solver" here means the algorithm used to solve a mathematical optimization program. Such simulation represents an expensive black-box objective function as viewed by the solver. The term "expensive" refers to the computational resources required to perform the simulation, which are significantly more than the resources required by the solver itself [38].

In optimization-based simulation studies, the parameters to be varied are changed in various manners such as with linear, logarithmic, or pseudo-random increments. This approach is wasteful in simulation time because no intelligence is used in determining the parameters for the next run based on the accumulated experience of the earlier runs [39].

2.5. Summary

Although optimization-based simulation studies provide accurate controller parameter values in the tuning process, they are mostly time-consuming and expensive in terms of the hardware requirements. This is particularly evident when the simulation case is complicated and includes a combination of LCC and VSC topologies or LCC-MMC ones. The cases can even be more complicated when multi-terminals exist in the network, each containing one or more LCCs. Such complex simulation cases require decent hardware (in terms of CPU and GPU) to run successfully, though they will still be time-consuming. To overcome this issue, a new simplified and fast model

of HVdc converters has been designed and developed in PSCAD/EMTDC to replace LCCs on either the inverter or rectifier sides. The new model can be used in place of the LCCs in various configurations such as purely LCC, LCC-VSC, and LCC-MMC on both rectifier and inverter sides of single or multi-terminal networks. This saves time when there is a need for multiple runs to tune the system's control parameters.

CHAPTER III

3. SYSTEM MODELING

Electromagnetic transient simulation programs (aka, emtp-type programs) are efficient tools to study, simulate and analyze the power networks [4]. Using these programs, users can obtain more precise and detailed results compared to other load flow and stability analysis programs [5]. In large networks, many simulation runs are usually needed to obtain the desired values for controller parameters. This is a time-consuming procedure when LCC-type converters are used in an HVdc system [1]. In this chapter, the mathematical modeling of LCC-based converters is explained followed by the procedure behind the implementation of the proposed HVdc converter model. The goal is to replace the existing 6-pulse bridge LCC model, currently used in PSCAD, with the proposed HVdc component to decrease the simulation time for complicated LCC-based networks.

3.1. Conventional LCC Model

The basic LCC configuration for HVdc uses a three-phase Graetz bridge converter (*i.e.*, 6-pulse bridge), having six thyristor valves, each connecting one of the three phases to one of the two dc terminals [13]. The LCC-based converters have their own advantages that make them a preferable configuration in HVdc power transmission. However, important points must be followed when modelling LCC-based converters, particularly by taking the grid control and overlap into consideration [13]:

- The injected power includes a balanced sinusoidal voltage and frequency connected in series with identical lossless inductances. Note that the main reason for the overlap is the presence of inductance, which primarily stems from the leakage inductance of the transformer.
- The dc current must be constant and ripple-free.
- The forward resistance of the valves is zero and their inverse resistance is infinite.
- The valves are ignited at equal intervals of 60 degrees, one-sixth of a cycle.

The 6-pulse Graetz bridge is the building block of an LCC-HVdc transmission system. Figure 3.1 shows the schematic of a 6-pulse Graetz bridge-based LCC converter considering a three-phase ac voltage source and a dc source. The block includes inductance (L_c) on the ac side to meet the requirement of continuity of currents in the ac source, as well as a smoothing reactor L_d to ensure the continuity of dc current.

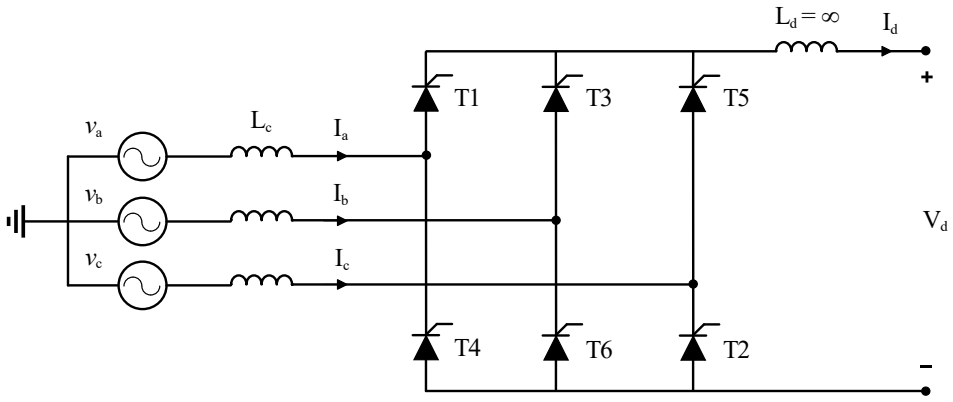

Figure 3.1 Schematic of 6-pulse Graetz bridge converter

3.2. AC Side Mathematical Formulation

The analytical modelling of the ac line, assuming the ac system is balanced, is expressed as follows [13]:

$$v_a = V_m \cos(\omega t + 60°) \tag{3.1}$$

$$v_b = V_m \cos(\omega t - 60°) \tag{3.2}$$

$$v_c = V_m \cos(\omega t - 180°) \tag{3.3}$$

where v_a, v_b and v_c are the ac voltage of phase a, b and c, respectively. V_m is the peak value of line-to-neutral ac voltage, and ω refers to the network frequency. Since the ac systems are assumed to be balanced, there is a $120°$ difference between phases. Subsequently, the corresponding line-to-line voltages are [13]:

$$v_{ac} = v_a - v_c = \sqrt{3} V_m \cos(\omega t + 30°) \tag{3.4}$$

$$v_{ba} = v_b - v_a = \sqrt{3} V_m \cos(\omega t - 90°) \tag{3.5}$$

$$v_{cb} = v_c - v_b = \sqrt{3} V_m \cos(\omega t + 150°) \tag{3.6}$$

where v_{ac}, v_{ba} and v_{cb} denote the line-to-line voltages. Based on Eqns. (3.1) - (3.6), the waveforms of instantaneous and line-to-line voltages are shown in Figure 3.2.

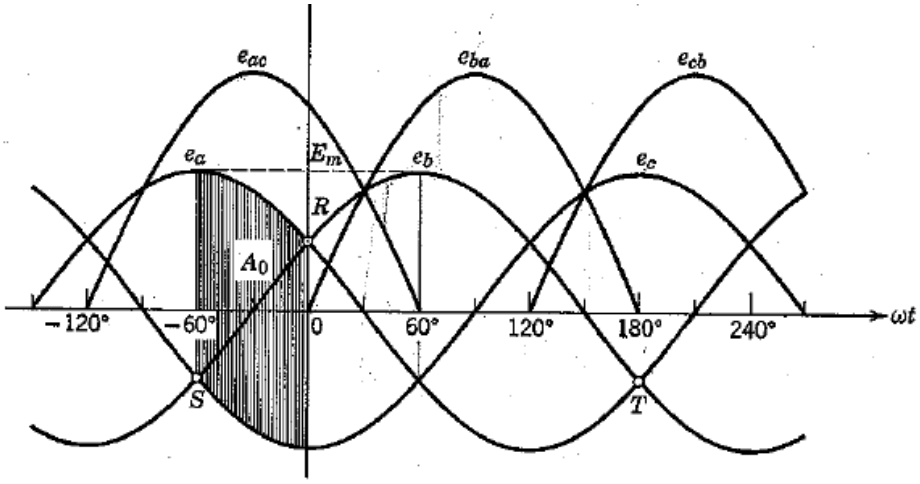

Figure 3.2 Waveform of instantaneous voltages of ac source: line to neutral, e_a, e_b, e_c; line to line, e_{ac}, e_{ba}, e_{cb} [13].

This model consists of six thyristors, fired sequentially with a delay angle known as α. Therefore, the thyristor is controllable by introducing the delay angle while diodes always exhibit a delay angle of zero. The delay angle corresponds to a time delay of α/ω seconds which is also called the firing angle. In LCC configurations, the connection to the bridge is made through a converter transformer, and thus, the inductance L_c is present between the source and thyristor valves [17]. As the current through the inductance cannot be changed instantaneously, there is a period during which all six valves conduct. This period is called the overlap angle μ [17]. Figure 3.3 illustrates the waveforms of the ac line-to-line voltages while the delay angle α is introduced to the thyristors. As can be seen in Figure 3.3, the overlap / conduction angle μ is also considered and its effect is visible on the ac current.

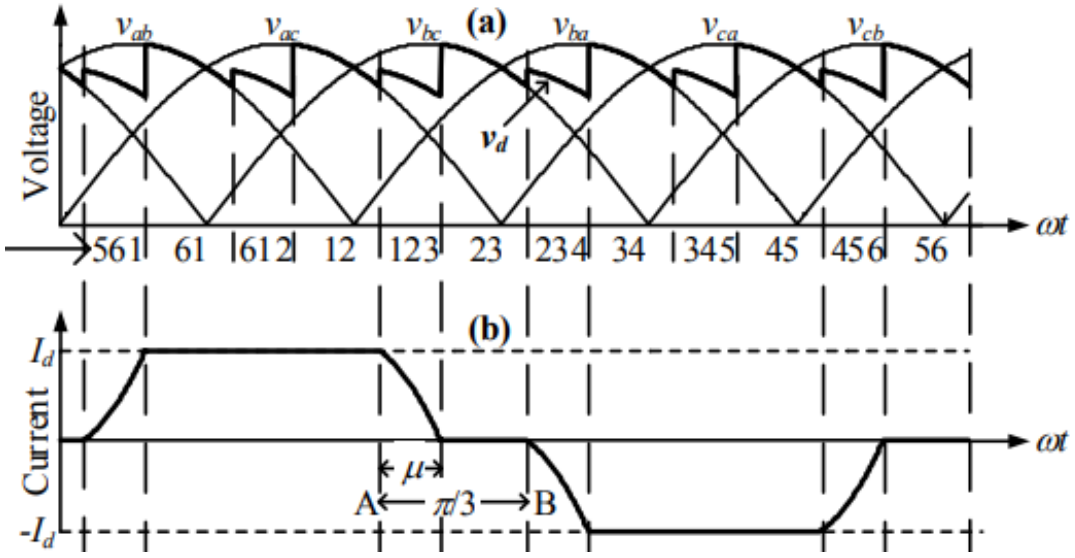

Figure 3.3 Line commutated converter waveforms. (a) three-phase line voltages and the dc voltage; (b) phase-a line current showing conduction angle [6].

It is noted that significant harmonics are generated by LCC converters due to the thyristor switching. Therefore, the smoothing reactor L_d is employed on the dc side of the converter to block the harmonics from entering the line. It also maintains dc current in the line and prevents lightning surge entering the converter in case of lightning.

3.3. DC Side Mathematical Formulation

On the dc side, the average direct voltage is determined by integrating the instantaneous ac voltages over any 60° period. For $\alpha = 0$ (no delay), and by having $\omega t = \theta$, the direct voltage is [13]:

$$V_{d0} = \frac{3}{\pi} A_0 = \frac{3}{\pi} \int_{-\frac{\pi}{3}}^{0} v_{ac}\, d\theta = \frac{3}{\pi} \int_{-60°}^{0} \sqrt{3}\, V_m \cos(\theta + 30°)\, d\theta = \frac{3\sqrt{3}\, V_m}{\pi} = 1.65 V_m \qquad (3.7)$$

where, A_0 is the integrating area between phase voltages v_a and v_c when θ changes from $-\frac{\pi}{3}$ to zero (see Figure 3.2). V_{do} is the ideal no-load direct voltage where the firing angle is zero. The average direct voltage can also be expressed in terms of rms line-to-neutral (V_{LN}) and line-to-line (V_{LL}) voltages [13]:

$$V_{d0} = \frac{3\sqrt{6}}{\pi} V_{LN} = 2.34\, V_{LN} = \frac{3\sqrt{2}}{\pi} V_{LL} = 1.35\, V_{LL} \tag{3.8}$$

In Eq. (3.7), if there is a delay angle α, both limits of integration are then increased by α, as follows [13]:

$$V_d = V_{d0} \int_{\alpha-60^\circ}^{\alpha} \cos(\theta + 30^\circ)\, d\theta = V_{d0} \sin(\theta + 30^\circ)|_{\alpha-60}^{\alpha} = V_{d0} \cos\alpha \tag{3.9}$$

According to Eq. (3.9), the ignition at the firing angle α in a converter reduces the amount of the average dc voltage by a factor of $\cos(\alpha)$. Since α can range from 0 to 180º, $\cos(\alpha)$ can vary from 1 to -1, and therefore, V_d will change from V_{d0} to $-V_{d0}$. Due to the unidirectional property of the valves, the direct current, I_d, cannot flow in reverse direction. Hence, the power reversal is achieved by reversing the voltage and firing angle of $\alpha < 90^\circ$, resulting rectifier operation. Consequently, the conjunction of V_d and I_d creates reversed power flow [13]. Because of this property, the inversion and rectification are defined based on the direction of the power flow. Note that the ripple and the harmonics in the dc voltage increase with the delay up to 90°, and then, decrease from 90° to 180°.

Neglecting the losses in the converter, the dc power and ac power must be equal and giving the following relationship [13]:

$$3V_{LN}I_{L1}\cos\phi = V_dI_d = I_dV_{d0}\cos\alpha \tag{3.10}$$

In Eq. (3.10), I_{L1} is the rms value of the fundamental frequency component of the ac line-to-neutral current, $\cos\phi$ is the displacement factor or power factor, and ϕ is the angle by which the fundamental line current lags the line-to-neutral source voltage. I_d represents the dc current which is obtained based on the leakage reactance X_c.

By Fourier analysis, the peak value of the fundamental component of this wave is [13]:

$$\sqrt{2}I_{L1} = \frac{2}{\pi}\int_{-\frac{\pi}{3}}^{+\frac{\pi}{3}} I_d\cos\theta'\,d\theta' = \frac{2}{\pi}I_d\sin\theta'|_{-60}^{+60} = \frac{2\sqrt{3}}{\pi}I_d = 1.103\,I_d \tag{3.11}$$

As a result of equality (3.11), the rms value of the fundamental current is obtained as follows:

$$I_{L1} = \frac{2\sqrt{3}}{\pi\sqrt{2}}I_d = \frac{\sqrt{6}}{\pi}I_d = 0.78\,I_d \tag{3.12}$$

Substituting Eqns. (3.8) and (3.12) into (3.10) yields:

$$\cos\phi = \cos\alpha \tag{3.13}$$

According to Eq. (3.13), if the firing angle α is zero, there is no phase shift between the dc voltage and the dc current. On the other hand, if there is a phase shift between the voltage and the current, the converter (either rectifier or inverter) draws the reactive power Q from the ac system. As a result, the rectifier always takes the lagging current from the ac system, while the inverter either takes the lagging current or delivers the leading current to the ac system [13]. This is equivalent to the definition of the type of converter when the firing angle is of concern, *i.e.*, the firing angle α is between 0° to 90° in a rectifier, while it is between 90° to 180° in an inverter.

3.4. Converter Control System

During disruptions, the stability and performance of the system relies on the prompt effectiveness of the control system significantly [40]. Incorporating special functions can improve the overall performance of the transmission system. If the ac network linked to the converter is strong enough (*i.e.*, high SCR and low impedance), designing a control system is straightforward and fast response is attainable; however, some exceptions may arise with lengthy ac cables or very long transmission line. On the other hand, if the converter links to a weak system (*i.e.*, low SCR and high impedance), extra effort is needed to achieve similar results as with a strong network [40].

In LCC configurations, current controllers are used to adjust the dc current to its setpoints. This is achieved by controlling the firing angle using a feedback control loop. As soon as the smallest possible value of α (α_{min}) is reached, the current controller is established when the desired value of current is obtained for any angle larger than α_{min} [6]. Under normal operating conditions, the rectifier operates in the current control mode, whereas the inverter operates in the extinction angle control mode. On the rectifier side, the dc current and dc voltage, in terms of the firing angle and leakage reactance, are obtained as follows:

$$I_d = (\cos(\alpha) - \cos(\alpha + \mu))\frac{V_{LL}}{\sqrt{2}X_c} \tag{3.14}$$

$$V_d = \frac{3\sqrt{2}}{\pi} V_{LL}\cos(\alpha) - \frac{3}{\pi} X_c I_d \tag{3.15}$$

where X_c is the leakage reactance of the transformer used between the ac source and the converter, and α is the firing angle. Also, μ is called the conduction angle and V_{LL} is the rms value of the line-to-line ac voltage. On the inverter side, the dc current and voltages are derived as follows:

$$I_d = (\cos(\gamma) - \cos(\gamma + \mu))\frac{V_{LL}}{\sqrt{2}X_c} \tag{3.16}$$

$$V_d = \frac{3\sqrt{2}}{\pi} V_{LL}\cos(\gamma) - \frac{3}{\pi} X_c I_d \tag{3.17}$$

In Eqns. (3.16) and (3.17), γ is the extinction angle and can be expressed as a function of the alpha order of the inverter side:

$$\gamma = \pi - (\alpha + \mu) \tag{3.18}$$

Note that the dc voltage and dc current formulated in Eqns. (3.16) and (3.17) are valid only if the three-phase ac system is balanced. In case of unbalanced ac voltages, the above equations are either approximate (for relatively small unbalances) or not valid. However, they are still useful for screening studies. The basic characteristic of a converter covering a range of full rectification to full inversion is illustrated in Figure 3.4.

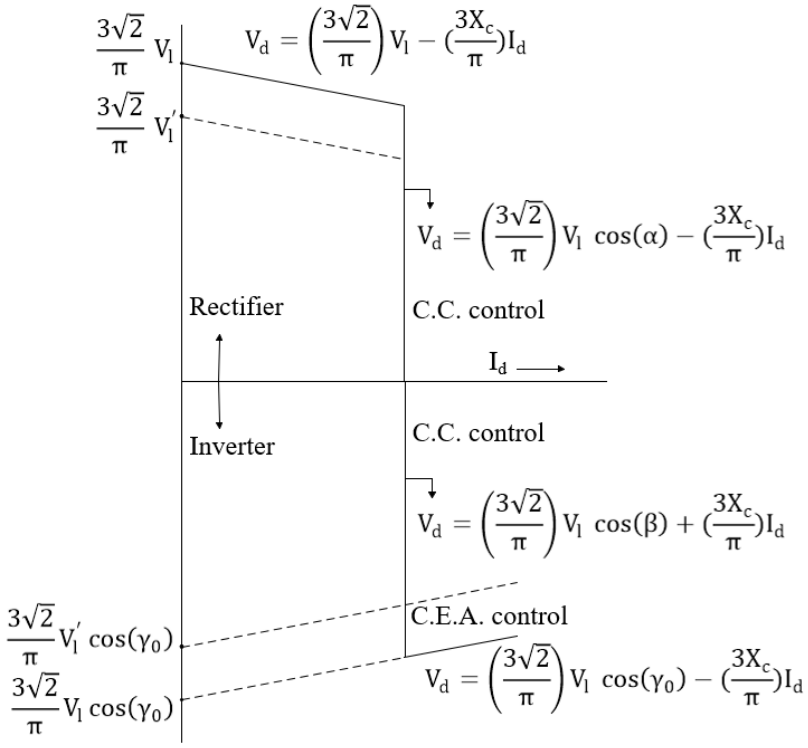

Figure 3.4 Complete control of a converter, from inversion to rectification [6].

As shown in Figure 3.4, for the firing angle greater than $\alpha = 0$ (on the rectifier side), or the extinction angle $\gamma > 0$ (on the inverter side), the converter employs constant current control, maintaining a current reference. These regions are governed by Eqns. (3.15) and (3.17). However, when the firing angle is zero, no further control is possible on the rectifier side, and the converter's V-I characteristic follows the natural voltage characteristic. On inverter side, the system is limited by the need to maintain a certain value of extinction angle (γ_0) which is the minimum amount for safe commutation when the value of the dc current is greater than the reference value [6].

3.5. New Fast and Simplified Model of HVdc Converters

This research focuses on the development of a fast and simplified HVdc converter model to replace LCCs in complicated schemes. The reason behind using the newly developed model is to speed up the process of tuning controllers' parameters in LCC-based HVdc simulation cases in PSCAD software. The presence of LCC decreases the speed of the simulation models significantly and can cause considerable delay in the tuning process. For simplicity, the newly developed model is, hereafter, called FS model (**F**ast and **S**implified model).

The principle behind the development of the FS model is to employ the steady state equations governing converters, *i.e.*, Eqns. (3.14) – (3.18) meaning that, the transient behavior of the HVdc models is not of concern, and the transient characteristics of LCCs are not studied in the process of developing the new model. The goal is to temporarily replace the 6-pulse bridge LCCs of complicated models with the FS model. The codebase used in the available scripts was modified to ensure the new FS model can play a similar role as the LCCs do in the steady state condition.

3.5.1. Structure of FS Model in PSCAD

To develop the FS model in PSCAD, a custom component was designed by considering three main sections in its Properties as “ac Side Configuration”, “dc Side Configuration” and “Converter Setting”, each responsible for setting values of the ac, dc and converter parameters according to the data taken from the original LCC-based model. There also exists a subsection called “Internal Output Variables” to defined required parameters to be used outside the FS component such as the extinction angle required as an input to the alpha controller on the inverter side. To distinguish between the converter types and allow the dc source to employ the corresponding formulations of either rectifier or inverter sides, a Boolean parameter was added, under the “Converter Setting”, to determine the rectifier or inverter type of the FS component.

The design procedure is fundamentally based on the measurement of dc current (I_d) on both the rectifier and inverter sides using multimeter components of the PSCAD master library; that is, two equations (3.14) and (3.16) are not used in the design process and the dependent variables such as the extinction angle and dc voltages are obtained from the measured dc current. Overall, the main input to the FS component is the alpha order (α), while the dc current (I_d) and the line-to-line ac voltage (V_{LL}) are inputted into the component internally. Figure 3.5 shows the overall graphic of two FS components, in series, to replace LCCs in HVdc models. The notation AO refers to the alpha order. To employ the FS component in lieu of the conventional LCCs in an HVdc case, one can simply remove the LCC components, located between the ac bus and the dc transmission line, and include the FS component in the HVdc model. Note that there is no need to remove the dc current controllers from the original model (*i.e.*, the AOR and AOI controllers of rectifier and inverter sides, respectively) as they need to be tuned in the entire model. Details on the structure of the FS component are explained in Chapter IV.

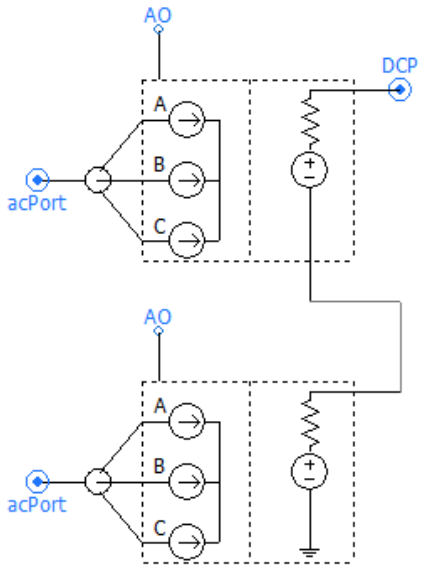

Figure 3.5 The overall graphic of FS component modelled in PSCAD. Two FS components are shown in series; "AO" means the alpha order and "DCP" is the dc port connected to dc transmission line.

Such a model is used in load flow stability studies which model the ac network in phasor form. It also does not consider the detailed switching behavior of the converter. However, the computational burden is much reduced, but it is not able to capture the higher bandwidth transients. In this thesis, we look at a hybrid approach where we use this model for the converter but represent the network in full EMT details. Thus, although the switching waveforms will not be precisely replicated, the overall dynamic response should still be accurate.

3.5.2. Formulation behind FS Model

According to Eqns. (3.14) and (3.15), the dc current and voltage of the rectifier side depend on the values of α and μ. However, as the inverter is normally operated with a constant extinction angle γ, it is more convenient to use Eqns. (3.16) and (3.17) on the inverter side which represents

the dc voltage and current as functions of γ and μ. As can be seen, the dc currents are dependent on the value of the conduction angle (μ). The dc current is internally measured using a multimeter component. To distinguish between the firing angle (α- order) of the rectifier and inverter, let us re-write the steady-state equations as follows:

For the rectifier side:

$$V_d = \frac{3\sqrt{2}}{\pi} V_{LL} \cos(AOR) - \frac{3}{\pi} X_c I_d \tag{3.19}$$

where, AOR means the alpha order of the rectifier side. For the inverter side, we have:

$$V_d = \frac{3\sqrt{2}}{\pi} V_{LL} \cos(\gamma) - \frac{3}{\pi} X_c I_d \tag{3.20}$$

where the extinction angle γ, can be expressed as a function of the current dc (I_d) from Eqns. (3.16) and (3.18):

$$\gamma = cos^{-1}\left(\left(\frac{\sqrt{2}X_c}{V_{LL}}\right) I_d + \cos(\pi - AOI)\right) = cos^{-1}\left(\left(\frac{\sqrt{2}X_c}{V_{LL}}\right) I_d - \cos(AOI)\right) \tag{3.21}$$

In Eq. (3.21), AOI is the alpha order of inverter side. It should be emphasized that the alpha order controller of the inverter side always requires an input of γ value. In the LCC model, the value of γ is outputted by the component itself as $\gamma_{measured}$. To ensure the functionality of the alpha controller is not affected by replacing LCCs with the FS component, the γ value is calculated from Eq. (3.21) and is defined as an output variable in the FS component.

Having calculated the value of γ from the measured I_d, and placing it inside Eq. (3.20), the dc voltage of the inverter side is obtained. On the rectifier side, the measured dc current from the rectifier dc port is used in Eq. (3.19) to find the values of the dc voltage at each time step. This

formulation is included inside a script of the FS component. Details of the implementation are explained in Chapter IV.

3.6. Summary

In this chapter, the mathematical formulation and behavior of HVdc systems were reviewed, and explanations on the types of controllers used for controlling the alpha orders on both the rectifier and inverter sides were provided. Given details about widely used LCC components in HVdc transmission systems, a newly developed fast and simplified model (FS component) of converters was introduced, along with the rationales behind the development of the new component in PSCAD. The overall structure of the FS component was explained, and the steady-state equations were reformulated to justify the design procedure based on the measurement of the dc current of both the rectifier and inverter sides.

Chapter IV

4. Implementation and Simulation Results

One of the features that makes the PSCAD a powerful EMT-based simulation software is its capability to enable users to customize their own component interfacing their own subroutines directly to the program [1], [41]. This chapter focuses on the design and implementation of the newly developed module (called FS component) to replace the detailed LCC models in PSCAD. First, steps of the design procedure are explained, and the FS component is used in simulation of the standard Cigre benchmark model. The comparison is conducted with detailed simulations using the standard PSCAD LCC component which models the switching behavior in detail. It is hoped that the model can be computationally faster, but nevertheless still able to capture the essential transient behavior.

Two LCC-based case studies, developed in PSCAD, are then introduced, followed by demonstrating the simulation results of both cases with and without the FS component. The

comparison is carried out to show the efficacy of the newly developed component in terms of (i) handling the commutation failure, and (ii) improving the simulation runtime.

4.1. Implementation of FS Component

To date, a wide variety of subroutines have been developed for each component modeling a certain part of a power system in the EMT simulator PSCAD. This way, the PSCAD library has been built up, enabling entire power system models to be constructed using a set of components related to HVdc, power electronics, FACT, or protection [1]. The proposed fast and simplified model also takes advantage of PSCAD capabilities to replace LCC components. The goal is to develop a component for the use in certain applications where an overall faster execution of a program is preferred over the more detailed valve group model of LCCs. The FS component is designed in a way to operate as a rectifier or an inverter of either polarity (see Figure 4.1). In the design procedure, the following criteria were considered:

(i) The dc side of the component is modelled as a dc voltage source employing Eqns. (3.19) and (3.21).

(ii) The ac side is modelled as a three-phase current source to interface the FS component to the ac side network.

(iii) The values of line-to-line ac voltage and the dc current (shown as VacRMS and Idc, respectively, in Figure 4.1) were measured from multimeter components of the PSCAD internally; that is, the multimeter is an internal part of the FS component, and there is no need to include extra multimeters beside the FS module when replacing LCCs.

(iv) The value of the extinction angle (γ) was defined as an internal output variable to be

used as an input to the alpha order controller of the inverter side. To obtain the extinction angle, Eq. (3.21) is used with two main inputs of the dc current and the inverter's alpha order.

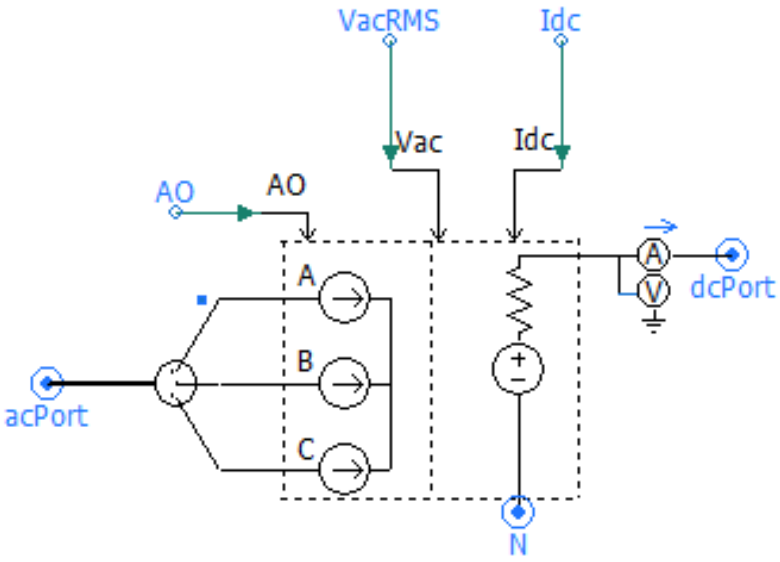

Figure 4.1 Overall schematic of FS component.

The codebase is embedded into the script section of the new component in PSCAD. In terms of the simulation, all runs have been carried out considering a time step of 50 μs or smaller, which is typical for modeling transients associated with LCC. This is because the proper operation of the program can be attained if the timestep is maintained below that of the smallest system time constant. For most systems that include converter station models, the smallest time constant is that of the valve group snubber circuit. The fact that modelling the actual switching action of thyristors usually requires the timestep to be less than 50 μs [1], led us to consider this amount for running the simulation model containing the FS component.

To replace the LCC component of an HVdc network with the FS model, it is required to remove the LCC component from the entire model and connect the acPort node of the FS model to the ac side and the dcPort to the dc transmission line (see Figure 4.1). In the next step, the parameters of the FS component are set according to the original model to ensure the proper data of the entire model is used in the replaced FS component. It is worth mentioning that any controller used in the original LCC model will remain unchanged, and only the LCC components will be replaced. For instance, the alpha order controllers existing on both rectifier and inverter sides will not be removed, and their output will be still used inside the FS component. To recall, the rectifier LCC adopts constant dc current control and minimum trigger angle control. Figure 4.2 shows the control block diagram of the LCC on the rectifier side of the HVdc system. To prevent the LCC commutation failure due to the low voltage during the fault, voltage dependent current order limiter (VDCOL) control is added to the rectifier LCC [21].

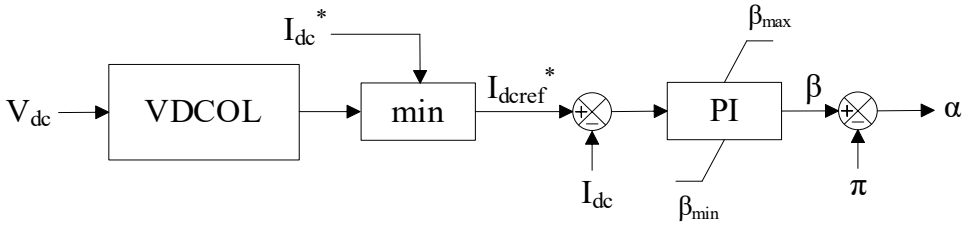

Figure 4.2 Control block diagram of LCC on rectifier side [21].

On the other side, the inverter LCC adopts constant extinction angle control and uses control and VDCOL control as backup control. The control block diagram of the inverter LCC is shown in Figure 4.3. To prevent the frequent switching between the constant extinction angle control and the VDCOL control, current error control (CEC) is added between the two controls [21].

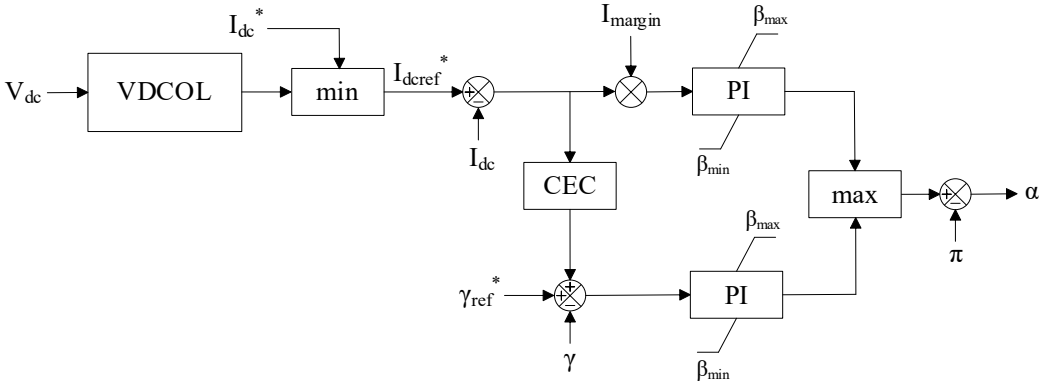

Figure 4.3 Control block diagram of LCC on inverter side [21].

4.2. Case Studies

In this research, two case studies were used to verify the performance of the newly developed component when replacing LCCs. Both cases contain two 6-pulse bridge LCCs on each side, rectifier and inverter.

4.2.1. Case Study I

In case study I, the Cigre benchmark model [42] was used. The benchmark model, which is a standard for understanding HVDC behaviour, represents a two-terminal monopole dc transmission system with two 6-pulse bridge converters in series. The rated voltage and transmission power is ± 500 kV and 1000 MW, respectively. The rated dc current is 2 kA. The actual short circuit ratios (SCRs) of the sending and receiving ends are both 2.5, and the effective SCR is 1.873 corresponding to a weak system. In the simulation, the rectifier control mode was constant-current, and the inverter control mode was constant-voltage [43]. Figure 4.4(a) demonstrates a schematic of the first Cigre HVDC Benchmark model, and Figure 4.4(b) shows the Cigre model using the proposed FS component.

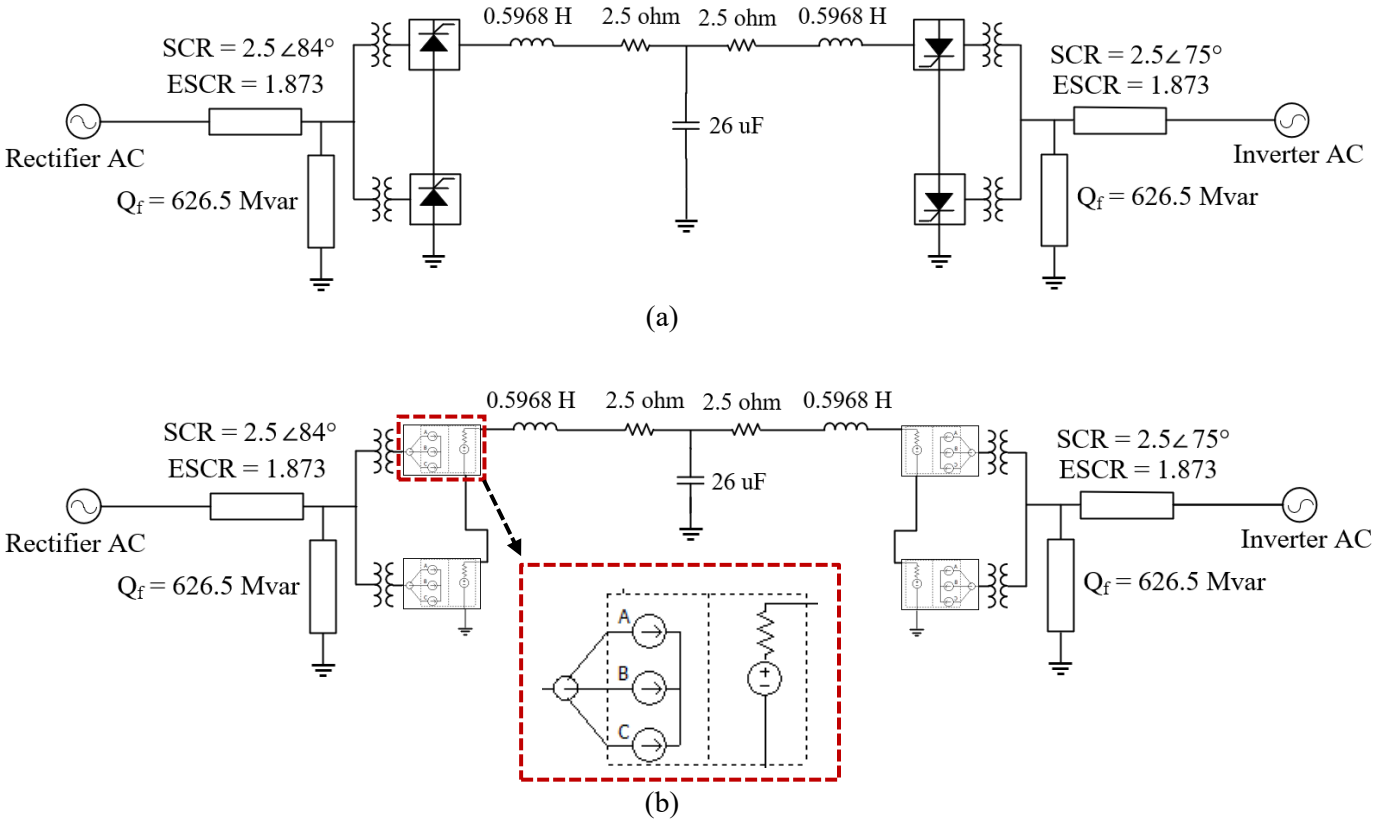

Figure 4.4 Schematic of Cigre benchmark model; (a) LCC model is used on both rectifier and inverter sides; (b) FS component is used.

4.2.2. Case Study II

In the second case study, another two-terminal dc transmission line is modeled with a rated dc voltage of 450 kV and is transmitting 840 MW power. The HVdc model contains a synchronous condenser on the inverter side. The dc current of the original LCC-based HVdc model is 1.85 kA. In this case study, a set of RLC filters are used on both rectifier and inverter sides to remove the 11^{th} and 13^{th} harmonics of the ac side. The case study includes two 6-pulse bridge LCCs, in series, on the rectifier and the inverter sides. Figure 4.5 shows a general view of this case study.

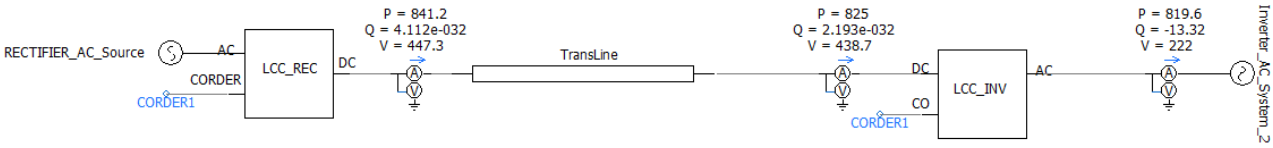

Figure 4.5 Schematic of Case Study II with a rated voltage of 450 kV and dc current of 1.85 kA.

4.3. Model Verification and Simulation Results

Having developed the FS component based on the steady-state equations governing LCCs and considering the design criteria mentioned in Section 4.1, the LCC component of the rectifier side was replaced by the FS module, and the detailed LCC model was retained on the inverter remained unchanged in the original Cigre benchmark model. A simulation was conducted with the rectifier side replaced by the FS component. The dc current (I_d) into the connected ac network was measured with an ammeter component and made available to the model for inputting into the controller which outputs the firing angle α as an input to the FS model. Knowing the dc current, the measured ac busbar voltage and the firing angle, the FS model can calculate the dc voltage and other internal parameters of the converter using Eq. (3.19). The simulation results are shown in Figure 4.6 which illustrates that the behaviors of the ac voltage, dc voltage and dc current have not changed when the FS component is used on the rectifier side. A comparison among the dc voltage and dc current of Figure 4.6 shows that both follow the dc voltage and dc current of the original LCC converter. This confirms that the FS model can produce similar steady-state results as what the detailed model does. Since the FS model cannot model the switching effects, the ripple caused by harmonics is not significant when the detailed LCC model is replaced by the simpler FS component. Note that the inverter side is still a detailed LCC model and will generate some harmonic ripples.

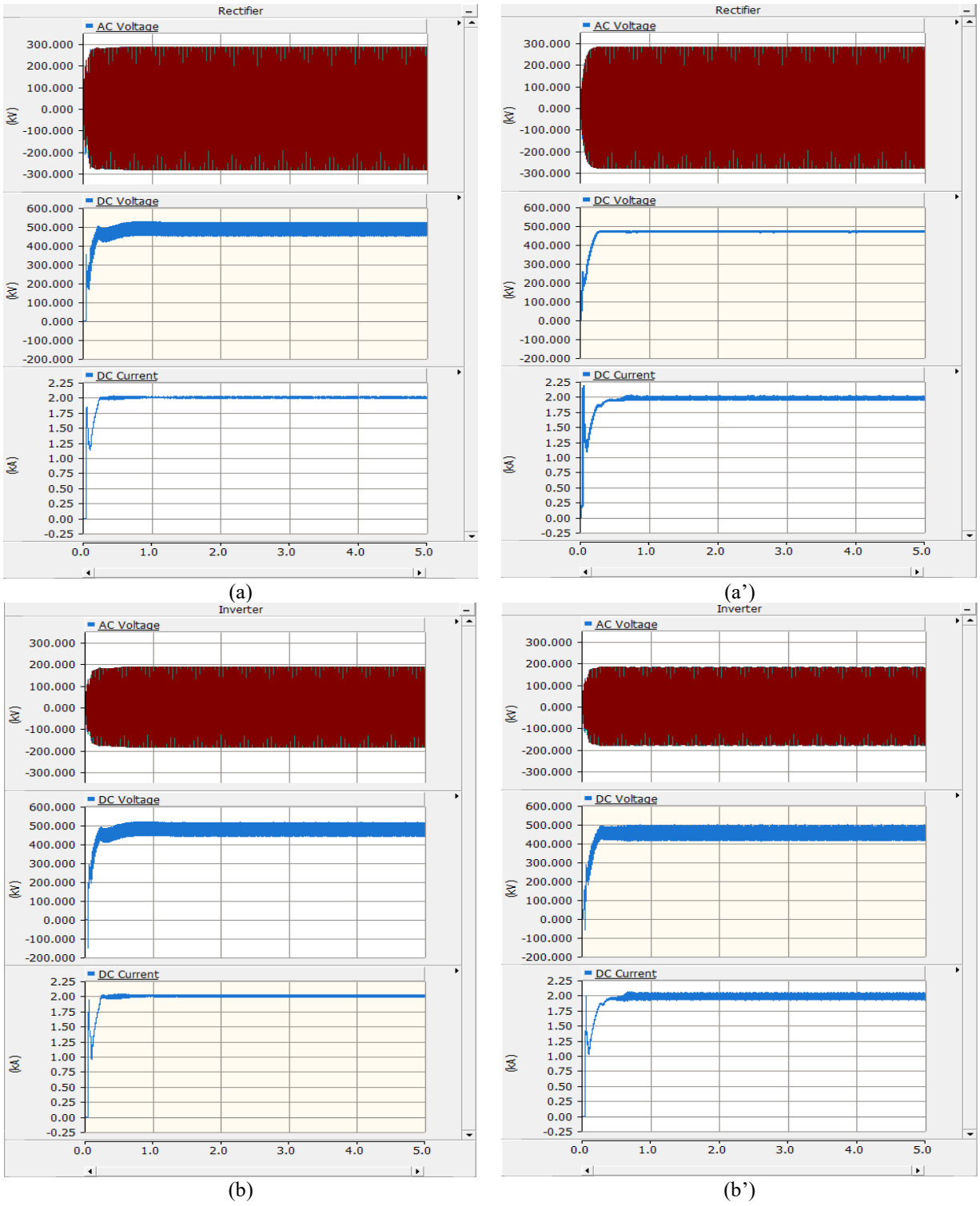

Figure 4.6 dc voltage and dc current of rectifier and inverter sides of the Cigre model. (a) and (b) Results of original Cigre model containing the detailed LCC model on both rectifier and inverter sides; (a') and (b') The FS component is used on the rectifier side only.

For further validation, we now replace all converters (rectifier and inverter) with the FS model. To implement the FS component in the given Case Studies, the ac lines were connected to the node "acPort" and the node "dcport" was connected to the dc line according to Figure 4.1.

First, the original model of Case Study I, with the detailed LCC models in PSCAD, was simulated and the ac voltages, dc voltage and dc current of the rectifier and inverter sides were observed. The results are shown in Figure 4.7(a) and (b) for both sides. As shown, both the dc voltage and dc current contain harmonics of high frequencies due to the switching phenomenon occurring in the detailed LCC components. Having replaced the LCC components with the FS component in Case Study I, the simulations results are reported in Figure 4.7(a') and (b'). A comparison of the dc voltage and dc current levels shows that results of the newly developed model are similar to those of the LCC component in steady state, and the ac voltages are not much affected by the new converter model. Also, as the FS model does not consider the individual thyristor valve switching, the 12^{th} harmonic ripple in the dc voltage and the dc current is not present. A detailed view of the results, in the steady state, shows that the dc voltage and current of the rectifier side approach their desired values, *i.e.*, ~ 470 kV and 2 kA on the rectifier side and ~ 460 kV and 2 kA on the inverter side. With respect to the ac voltages, a comparison demonstrates that the drop in the ac voltage value, from the rectifier side to the inverter side, follows a similar pattern whether the LCC or the newly developed FS component is used. The main difference in the behavior of the dc voltage and current is observed in the transient period which is due to the fundamental difference in the operation of the LCC and the FS component. Also, there exists a voltage and current drop between 0.3 seconds and 1.0 seconds in the FS model as shown by red ellipses on Figure 4.7.

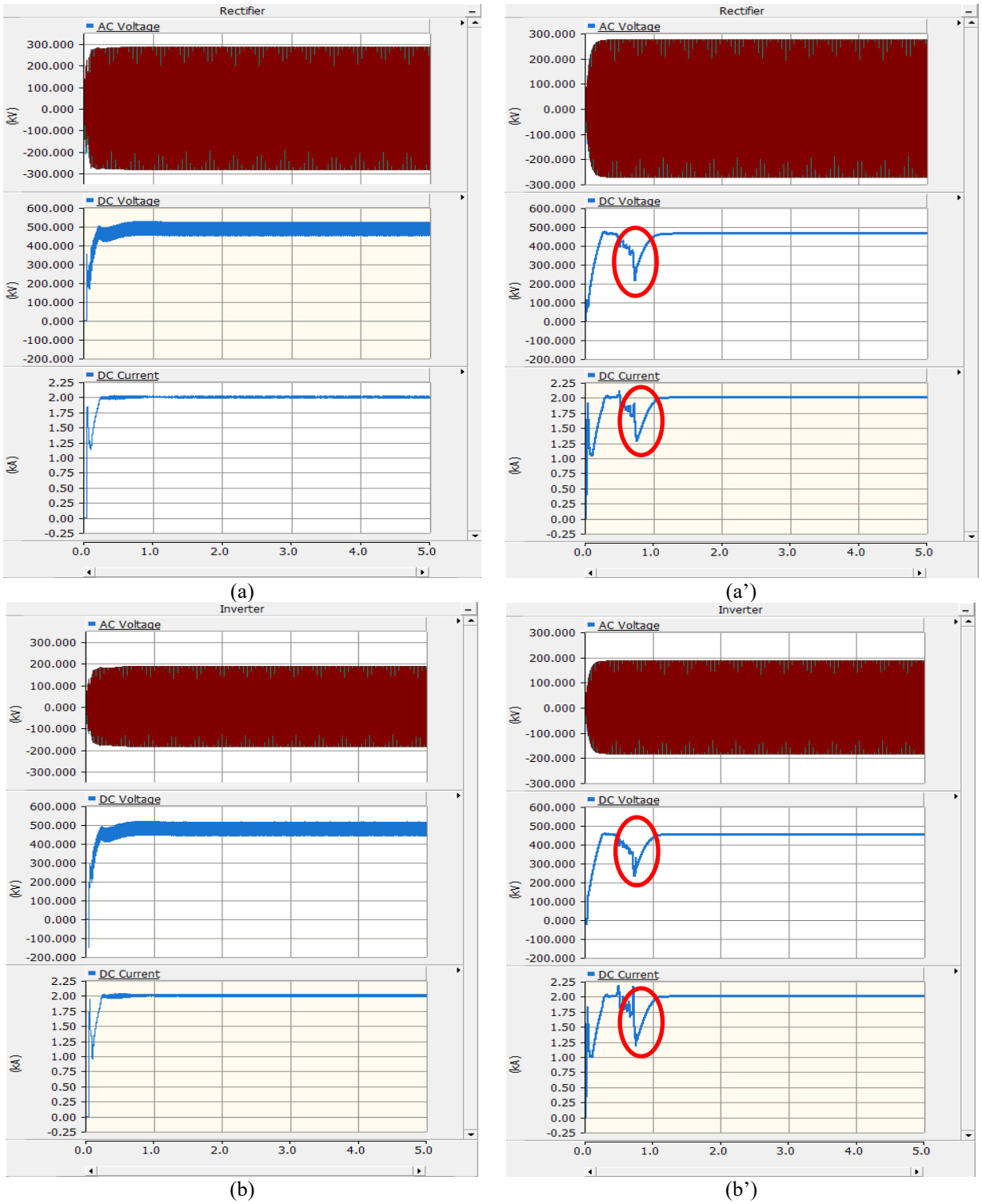

Figure 4.7 Case Study I: ac voltages, dc voltage and dc current of rectifier and inverter sides; (a) and (b) detailed model with two 6-pulse bridge LCCs. (a') and (b') All LCCs are replaced by FS components.

The drops, shown in Figure 4.7, are because of the FS model appears to be very sensitive to the gains TF1 = 0.002 and TF2 = 0.5 in the inverter controller of the original Cigre model (Figure 4.8). Modifying these gains marginally to TF1 = 0.0025 (by 25% increase) and TF2 = 0.55 (10% increase) eliminates this problem.

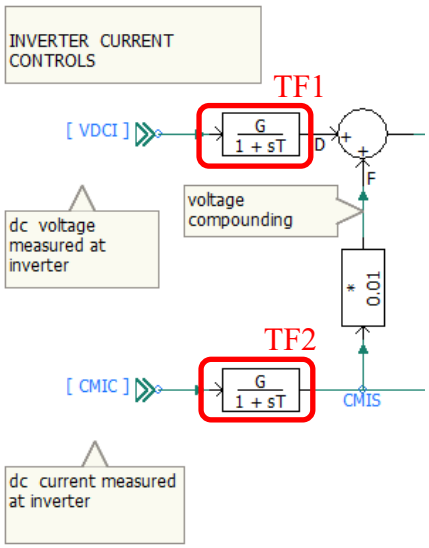

Figure 4.8 A closeup view of two blocks used in inverter controller of original Cigre model.

The modified results based on the new gains are shown in Figure 4.9. As can be seen, there are no longer drops between 0.3 and 1.0 seconds in the dc voltage and dc current behaviors, and both dc voltage and dc current reach their steady-state value at around 0.3 seconds. The corresponding behavior of firing angles of the rectifier and inverter and the inverter's extinction angle is shown in Figure 4.10.

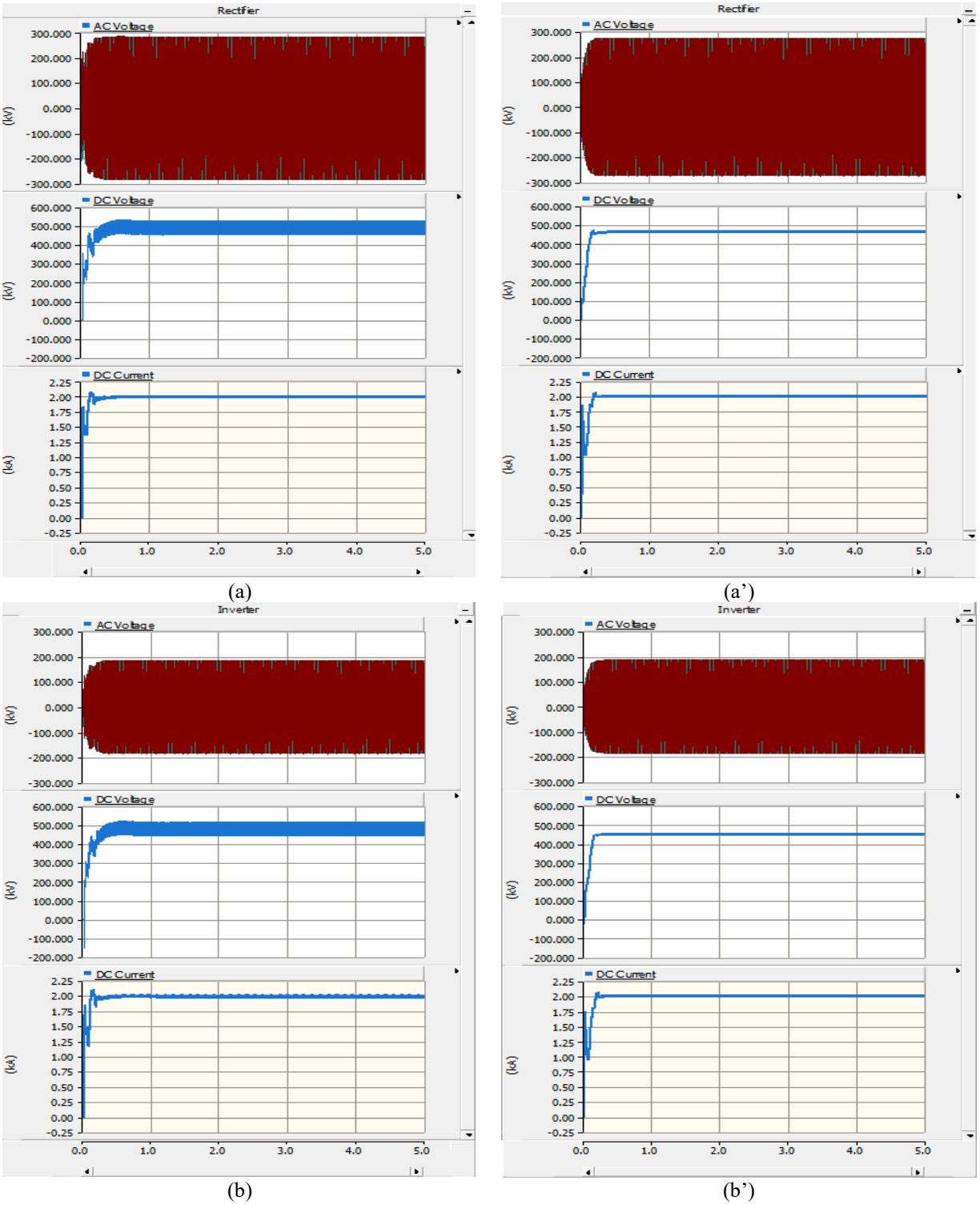

Figure 4.9 Case Study I: simulation results based on new gains used in inverter controller; (a) and (b) detailed model with two 6-pulse bridge LCCs. (a') and (b') All LCCs represented by FS components.

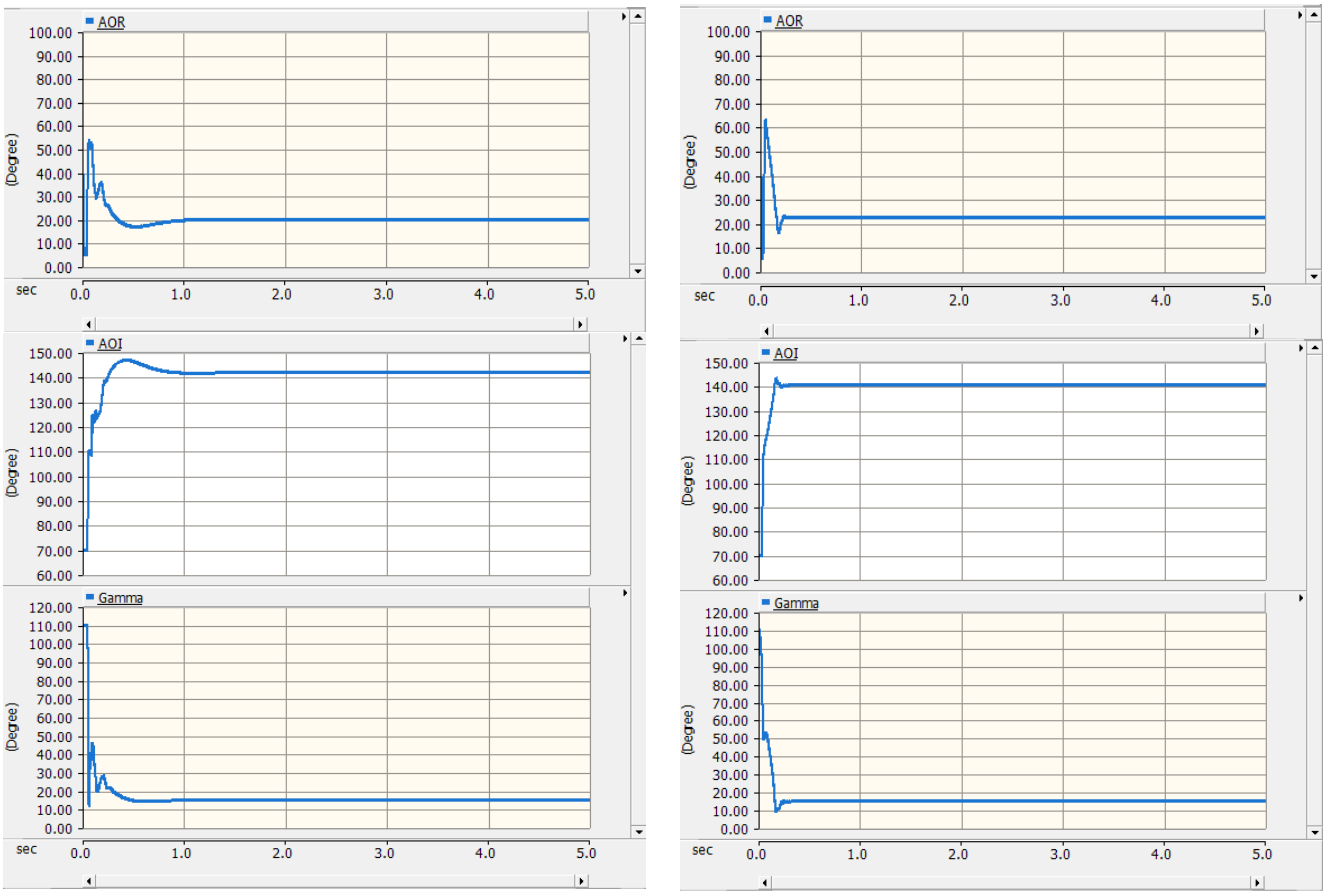

(a) (b)

Figure 4.10 Case Study I: rectifier alpha order (AOR), inverter alpha order (AOI) and extinction angle (Gamma) based on new gains of inverter controller; (a) two 6-pulse bridge LCCs are used. (b) FS components are used on both sides.

For the Case Study II, a similar comparison was carried out by replacing LCCs of the rectifier and inverter sides with the FS component. Figure 4.11(a) and (b) demonstrate the simulation results when the original LCC components are used. As shown in Figure 4.11, the dc voltage contains high frequency oscillations due to the presence of LCC components. This is while these oscillatory behaviors are not observed when the FS component is utilized on both rectifier and inverter sides [see Figure 4.11(a') and (b')]. In addition, the dc voltage and dc current reach their desired values (*i.e.*, ~ 450 kV and 1.85 kA on the rectifier side and ~ 440 kV and 1.85 kA on the inverter side) when the FS model is used.

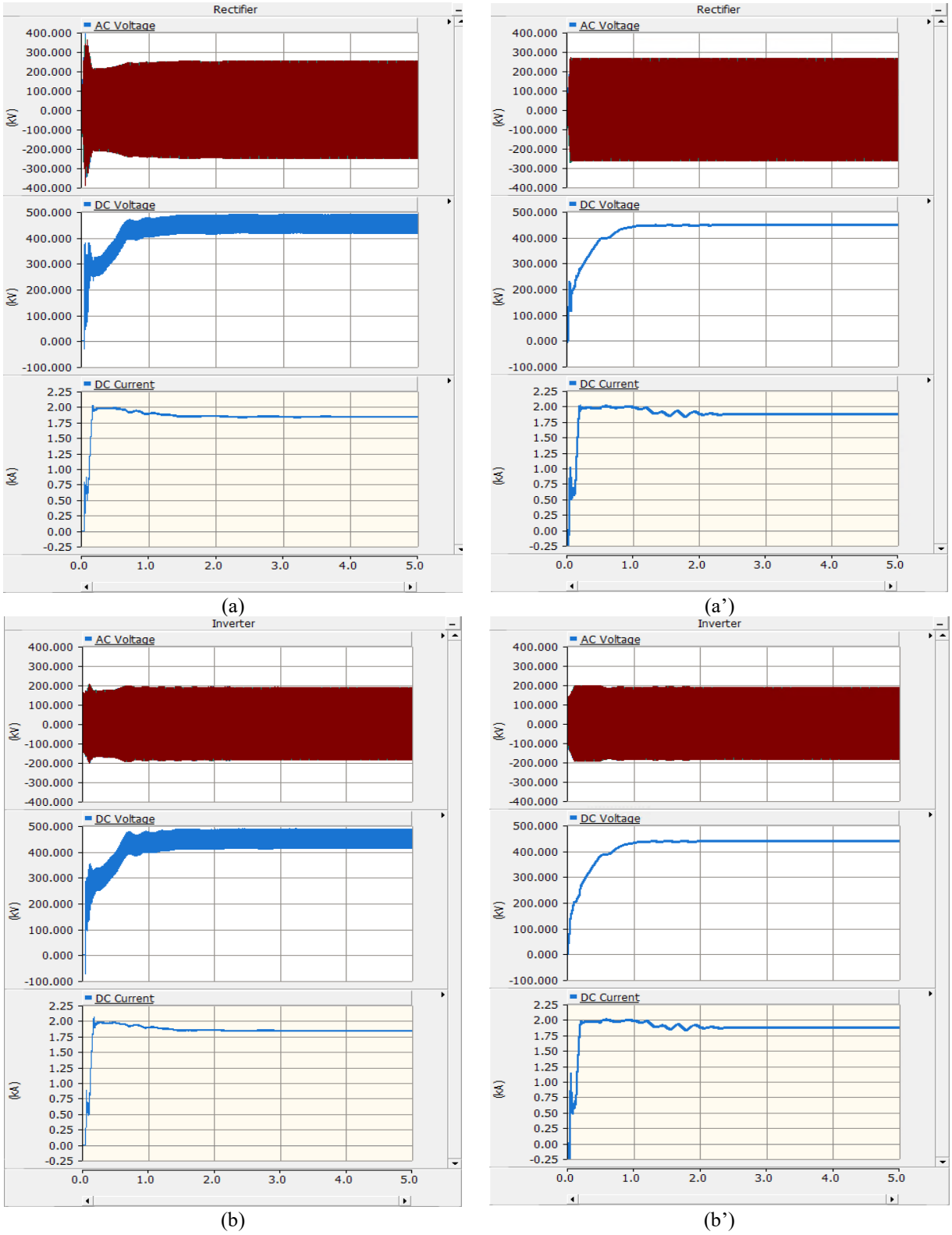

Figure 4.11 Case Study II: ac voltages, dc voltage and dc current of rectifier and inverter sides; (a) and (b) two 6-pulse bridge LCCs are used. (a') and (b') and FS components are used on both converter sides.

Like Case Study I, the implementation of the FS model in the given HVdc model does not affect the behavior of the entire model on the ac side as the ac voltages are essentially the same in both LCC-based and FS-based models. The comparison between the alpha orders and the extinction angles of both scenarios on Case Study II is also shown in Figure 4.12. As shown, the alpha orders and the extinction angle behave similarly when either the LCCs or the FS components are used in the HVdc model.

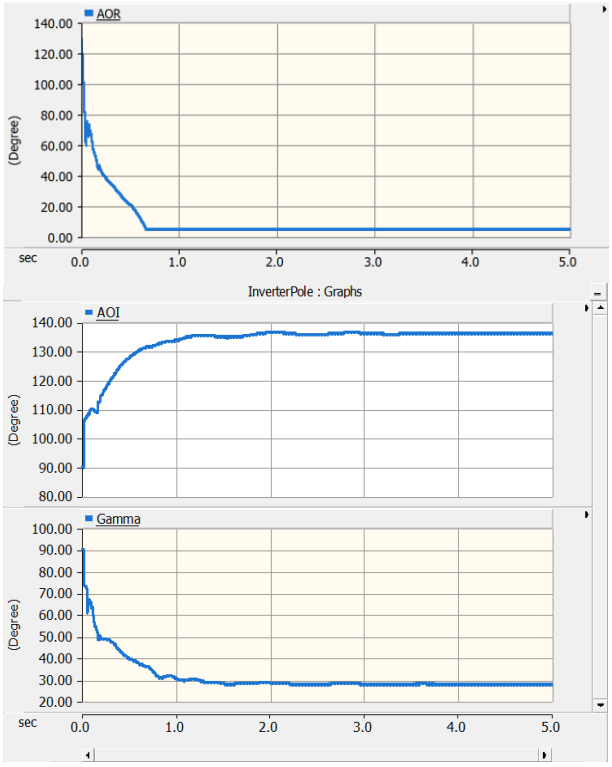

(a)

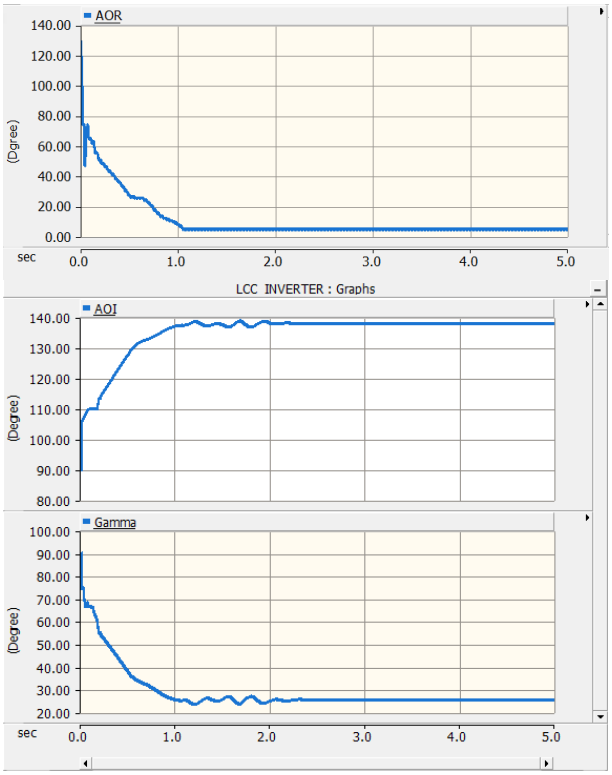

(b)

Figure 4.12 Case Study II: rectifier alpha order (AOR), inverter alpha order (AOI) and extinction angle (Gamma); (a) two 6-pulse bridge LCCs are used. (b) FS components are used on both sides.

The above comparisons revealed the fact that the FS component could be a suitable candidate for the LCCs when controller parameters tuning is of concern. All simulation results showed that

the replacement of the LCC modules with the FS component did not affect the behavior of the system parameters on both the ac side and dc side, in the steady state, compared to the scenario of using the original LCCs.

To investigate the efficacy of the newly developed component representing the effect of a commutation failure, a new set of simulations was conducted. As is known, commutation failure occurs due to a disturbance in the ac system mostly because of a voltage drop or the occurrence of a fault near the inverter. To simulate the commutation failure, a symmetrical three-phase fault was applied near the ac bus of the inverter at time t = 2.5 *sec* for a duration of 100 *msec*. The first set of results is shown in Figure 4.13 illustrating how the ac voltages and dc voltage and dc current are affected by the fault in both LCC-based and FS-based models. The behavior of firing angles and the extinction angle when the FS component is used in place of LCCs are also shown in Figure 4.14(a') and (b'). Although the commutation failure caused by the ac fault is not precisely modelled and is only approximated, comparing the results taken from the original Cigre benchmark model (left columns of Figure 4.13 and Figure 4.14) and those of the FS component (right columns of Figure 4.13 and Figure 4.14) confirms that the newly developed component can still handle commutation failure and recovers the ac voltages and dc voltage and current with reasonable accuracy. In FS-based Cigre model, the dc voltage drops sharply almost 30 *msec* after the fault inception and is then fully recovered at time t ≅ 3.1 *sec* (which is about 500 *msec* after the fault). With respect to the original LCC-based Cigre model, the full recovery from the fault occurs at t ≅ 3.2 *sec*. The difference in the recovery time between two models is because the detailed waveforms, during the fault, do not agree precisely due to the reduced ability of the FS component to represent phenomena such as commutation failure.

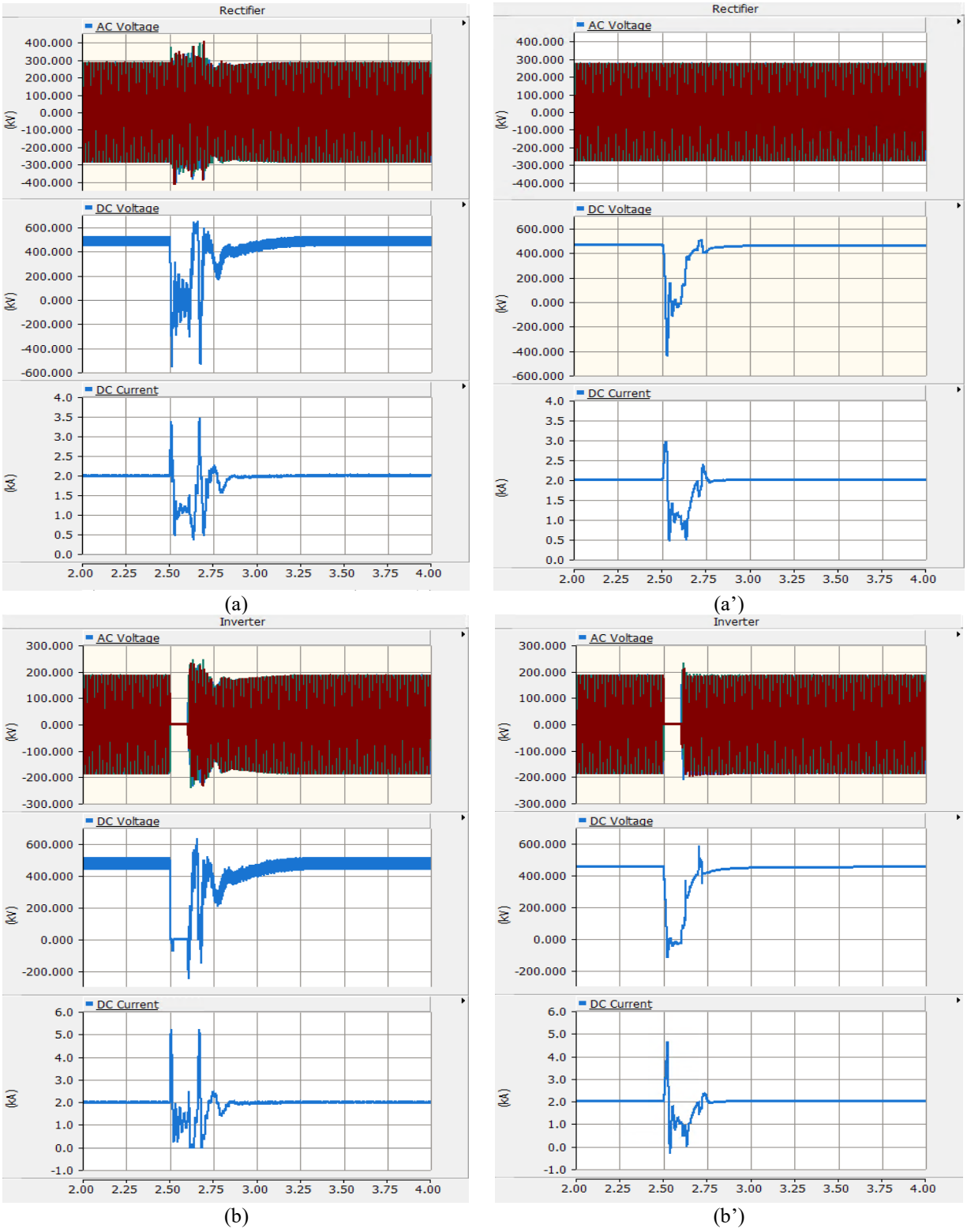

Figure 4.13 Case Study I with Commutation Failure at t = 2.5 seconds: ac voltages, dc voltage and dc current of rectifier and inverter sides; (a) and (b) detailed model with two 6-pulse bridge LCCs. (a') and (b') All LCCs represented by FS components.

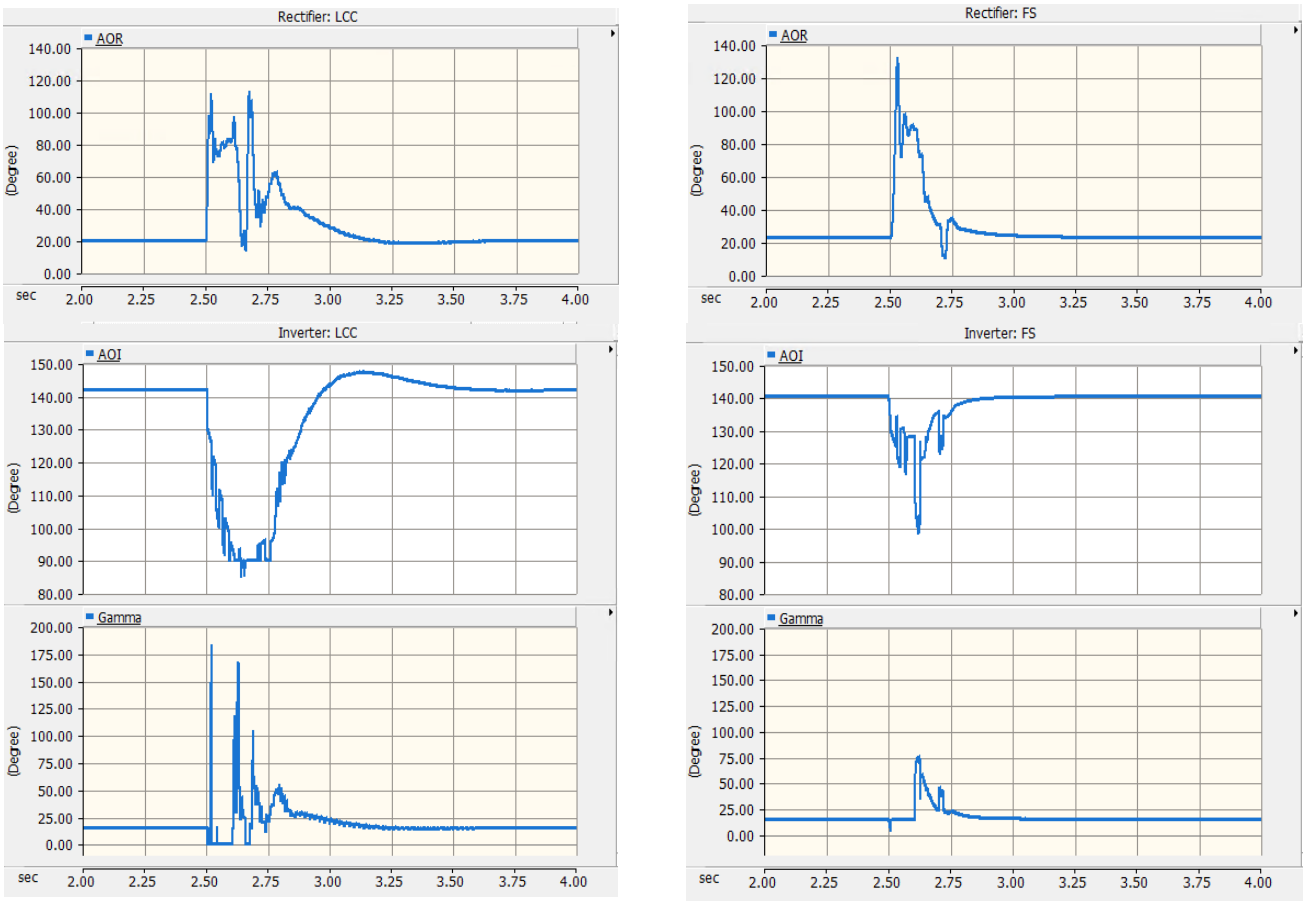

(a) (b)

Figure 4.14 Case Study I with Commutation Failure as t = 2.5 seconds: rectifier alpha order (AOR), inverter alpha order (AOI) and extinction angle (Gamma); (a) two 6-pulse bridge LCCs are used. (b) FS components are used on both sides.

To investigate the power recovery after the fault occurrence, another set of simulation results was obtained by comparing the behavior of the dc powers on both rectifier and the inverter sides. As shown in Figure 4.15(b), the FS component can recover the dc powers of both rectifier and inverter sides to more than 90% of the pre-fault values within ~130 *msec* after the fault inception (at t ≅ 2.73 *sec*), confirming that the simplified model (*i.e.*, FS component) could be valid for such screening studies.

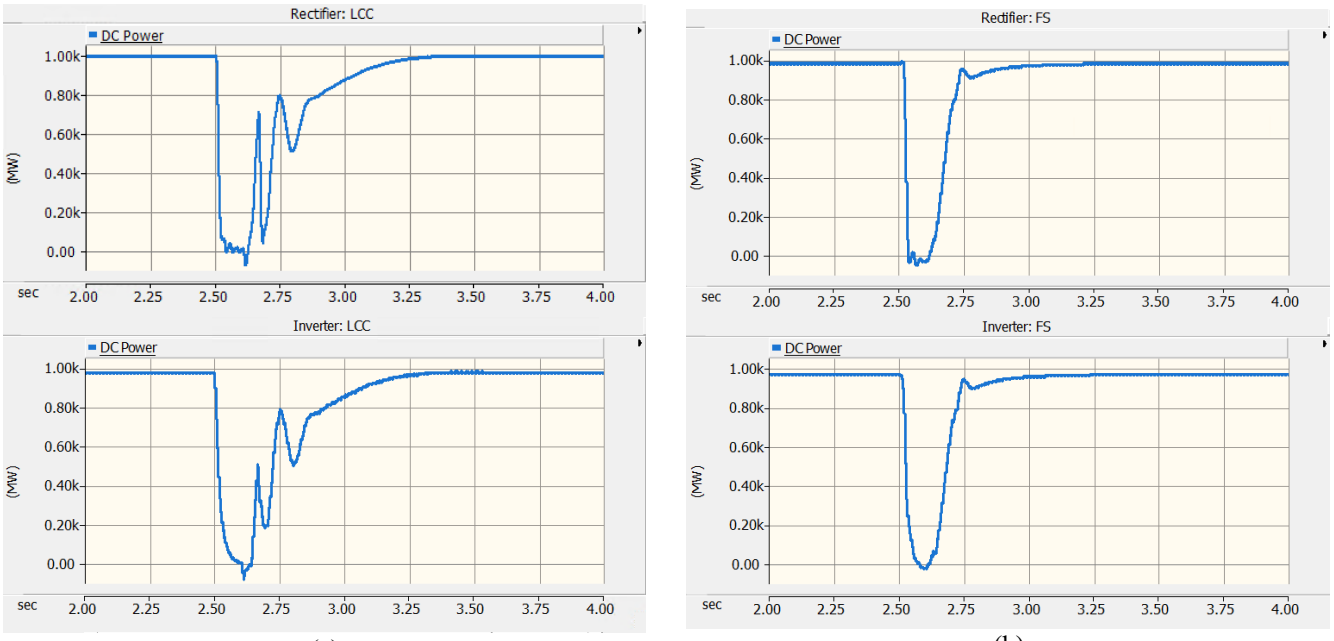

(a) (b)

Figure 4.15 Case Study I with Commutation Failure as t = 2.5 seconds: behaviors of dc power of both rectifier and inverter sides during the fault; (a) two 6-pulse bridge LCCs are used. (b) FS components are used on both sides.

A similar simulation study was conducted on Case Study II which includes a synchronous condenser and has a smaller power rating (840 MW) than the Cigre benchmark model (1000 MW). The same three-phase fault was applied near the ac bus of the inverter in Case Study II. The first set of results is demonstrated in Figure 4.16 where the fault is applied at time t = 2.5 *sec* for a duration of 100 *msec*. As can be observed, the ac voltages, dc voltage and dc current are recovered at almost the same time (t ≅ 3.2 *sec*), in both FS-based and LCC-based models, demonstrating more agreeable results compared to those of Case Study I. However, the detailed waveforms of the current and voltages are not the same, during the fault, in both models, which indicates the limitation of the FS component in simulating the commutation failure precisely.

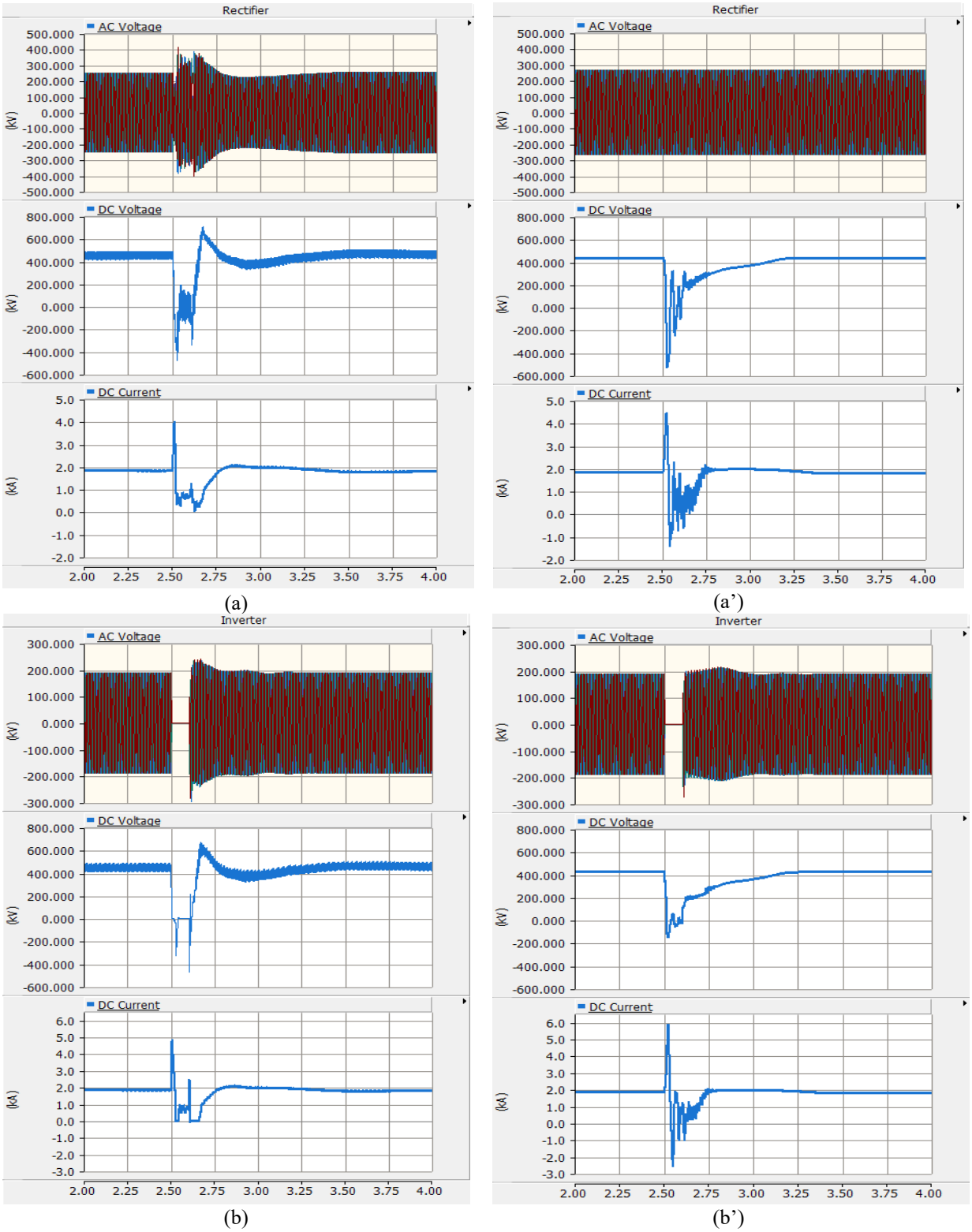

Figure 4.16 Case Study II with Commutation Failure at t = 2.5 seconds: ac voltages, dc voltage and dc current of rectifier and inverter sides; (a) and (b) detailed model with two 6-pulse bridge LCCs. (a') and (b') All LCCs represented by FS components.

The behavior of the dc powers was also investigated, in Case Study II, during and after the fault with the results are shown in Figure 4.17. Like Case Study I, the FS model can recover the power after the fault. In both the FS model and LCC model of Case Study II, the dc powers of the rectifier and inverter sides reach 90% of their pre-fault value at around t ≅ 3 *sec* confirming that the FS model could be a suitable candidate for the LCCs in screening studies.

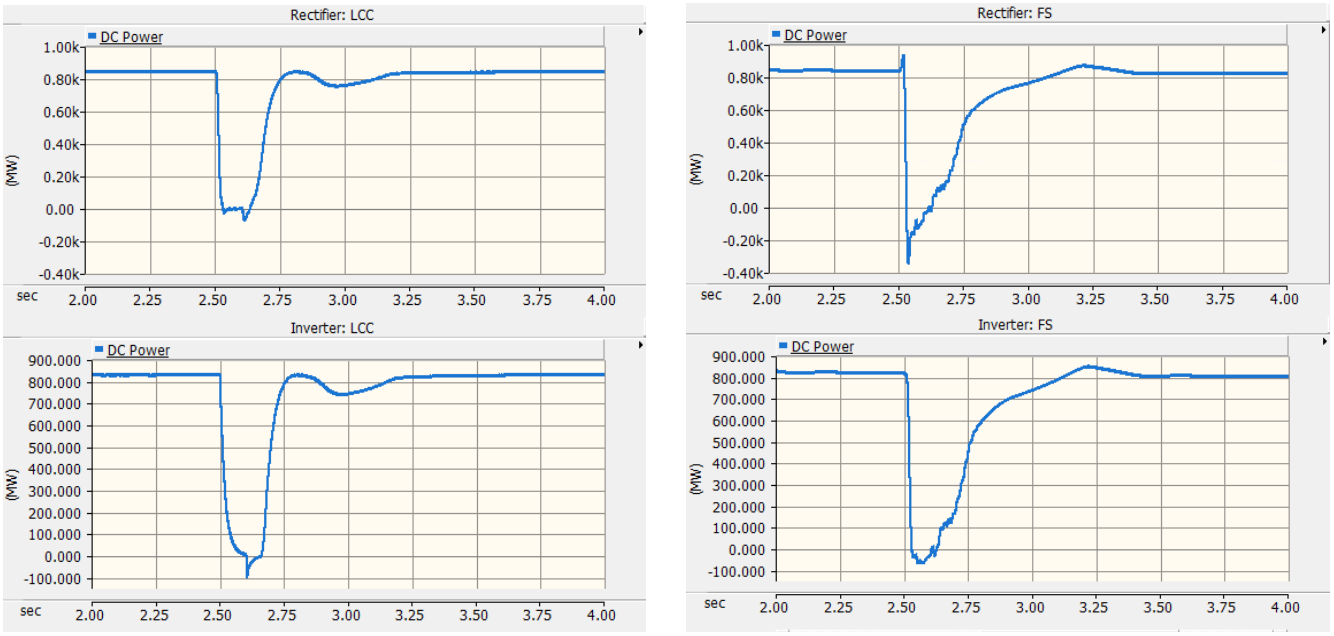

(a) (b)

Figure 4.17 Case Study II with Commutation Failure as t = 2.5 seconds: behaviors of dc power of both rectifier and inverter sides during the fault; (a) two 6-pulse bridge LCCs are used. (b) FS components are used on both sides.

Figure 4.18 also shows the changes in behaviors of the firing angles and the inverter extinction angle during the fault occurrence. As shown, the angles are fully recovered after the fault is cleared. With respect to the rectifier firing angle, the angle immediately jumps to about 140°, and then starts to decrease back to its original value (~ 5°), in both models, within 700 *msec*. This is while

the inverter alpha angle drops to its minimum value (~ 110°), remaining unchanged for ~ 200 *msec* and then increasing to its original value (~ 136°) at t ≅ 3.2 *sec*. The amount of the variation for the extinction angle, during the fault, is different in both models, having a considerable jump to ~ 300° in LCC-based model whereas the same angle does not exceed 150° in FS-based model of Case Study II.

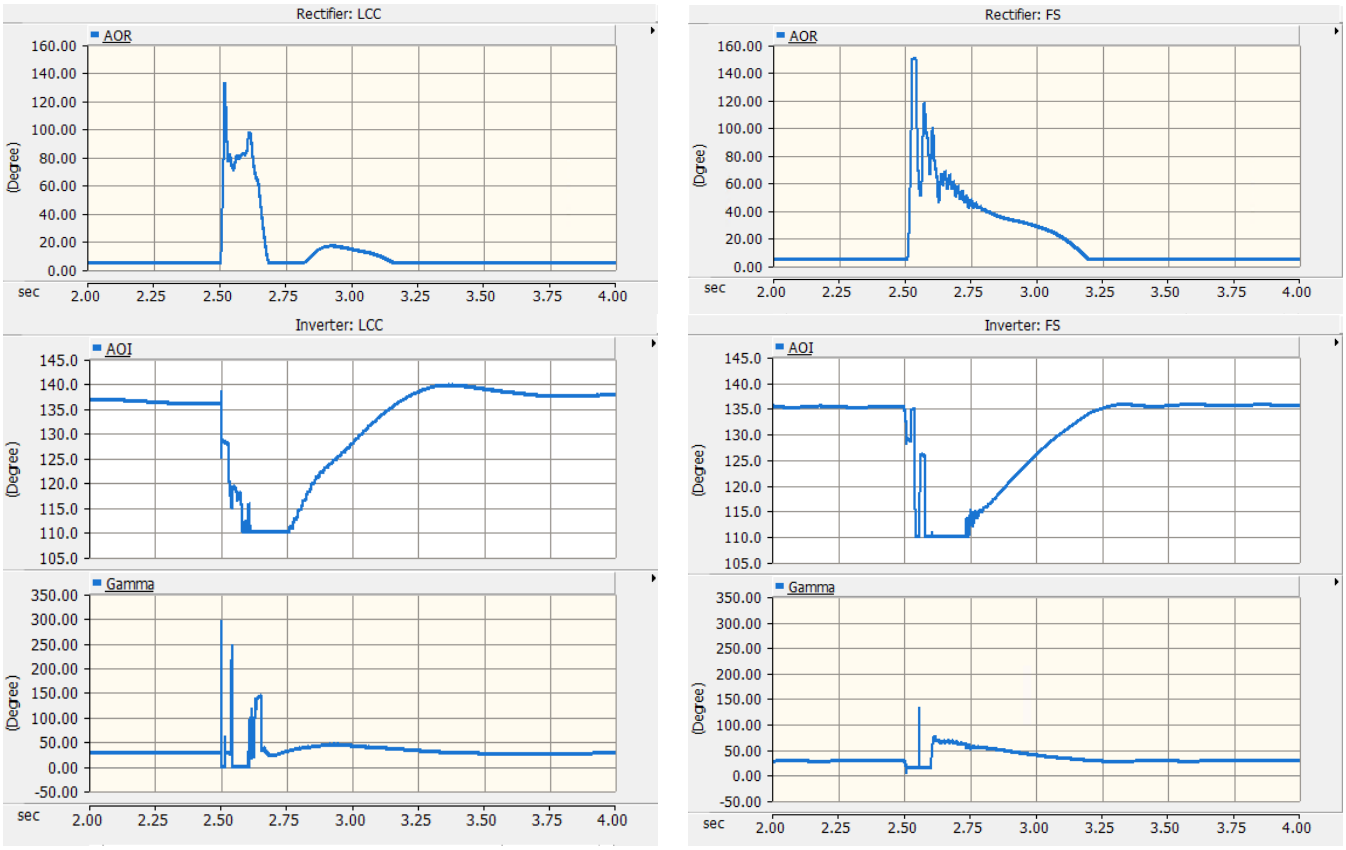

(a) (b)

Figure 4.18 Case Study II with Commutation Failure as t = 2.5 seconds: rectifier alpha order (AOR), inverter alpha order (AOI) and extinction angle (Gamma); (a) two 6-pulse bridge LCCs are used. (b) FS components are used on both sides.

Finally, both case studies were run in two scenarios, one with LCC and the other with FS component, to find out the difference between the actual simulation times. To do so, the .map files

of the simulation runs were used for the execution, and the real-time runs were calculated using a Python code with the results shown in Figure 4.19. In both HVdc models comprising the FS component resulted in faster simulation runs. Note that the period of the PSCAD simulation time was set to 3 seconds for all cases; however, the actual runtime is always more than the simulation time. As shown in Figure 4.19, the real-time simulation run for Case Study I with LCC component is around 13 seconds, while the corresponding value for the same case study with FS component is 4 seconds. In Case Study II, the run times for LCC-based and FS-based models are 20 seconds and 9 seconds, respectively, which reveals how faster the HVdc models are run using FS components.

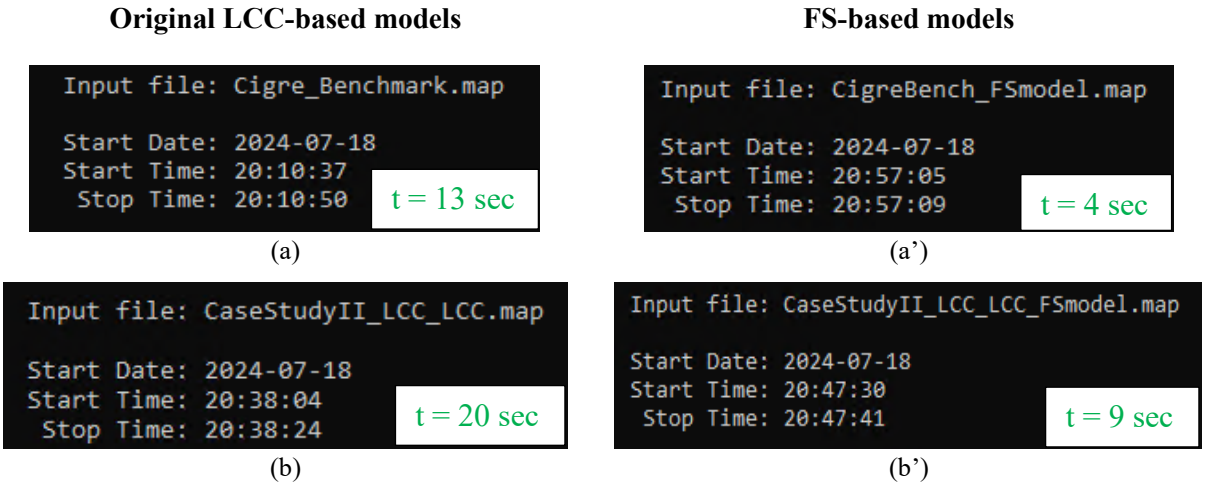

Figure 4.19 Comparison of real-time simulation runs between LCC-based and FS-based models; (a) result of running Case Study I with LCC; (a') result of Case Study I with FS model; (b) and (b') are real-time simulation runs for Case Study II with LCC and FS models, respectively.

4.4. Summary

This chapter focused on the implementation of the FS component along with the demonstration of simulation results for two Case Studies. First, the design criteria behind the development of the

FS model were explained followed by a brief introduction of two Case Studies. A model verification was conducted by replacing LCCs of only the rectifier side with the newly developed component. The results showed that the FS component could operate properly along with the LCCs located on the inverter side in the Cigre benchmark model. Further Simulation results and comparisons were carried out to ensure the efficacy of the FS component when all LCCs on both the rectifier and inverter sides are replaced. Moreover, a set of simulations was conducted to find out if the FS component can handle the commutation failure.

Based on the results, the FS component showed a capability to replace LCCs for screening studies as the system parameters including the ac voltages, dc voltage and dc current as well as the alpha and extinction angles could follow a similar trend as those of LCCs in the steady state. Also, it was found that the FS component could handle commutation failure and recover the voltages and currents, after the fault, in a similar manner as how LCCs do. In addition, the investigation on the dc power recovery indicated that the FS model could successfully recover the dc powers of both rectifier and inverter sides to more than 90% after the fault is cleared. However, the detailed waveforms of voltages, currents and angles do not exactly match which is due to the reduced ability of the FS component to represent phenomena such as commutation failure.

Finally, a comparison between the actual runtime of the simulations was made. The results proved the efficacy of the FS component in speeding up the simulation runs more than two times compared to when the LCCs are used in the original models. This result can be noticeable for complicated models where tuning of several control parameters is of concern. The developed FS component could, therefore, have the potential to be used for screening studies in PSCAD.

CHAPTER V

5. CONCLUSIONS

With the aim of accelerating the simulation time for newly developed PSCAD cases in HVdc networks, there is a need to develop fast-responding components. In this research, a fast and simplified converter model was designed and developed, in PSCAD, to replace LCC modules in HVdc cases. Overall, this study intended to contribute to reducing the actual simulation time in HVdc models during the process of controller parameters tuning while maintaining the accuracy of the overall dynamic response.

5.1. Thesis Contribution

In this thesis, the steady-state equation governing HVdc converters, either rectifier or inverter, were employed to develop a fast and simplified model of a converter. In developing the new component, the following contributions were made:

(i) A new component simulating an HVdc converter was designed and developed in PSCAD. The component comprises a set of parameters to address the required settings for both ac and dc side, as well as the converter's parameters. The design was made in a way to simplify the process of replacing any LCC component with the newly developed model. During the design process, efforts were made to avoid the removal of LCC-dependent components used in complicated HVdc models. To emulate the functionality of LCCs using the new component, the steady-state governing equations on LCCs were coded in the script section of new component along with defining a set of internal output variables to maintain the consistency of the component with other modules/ blocks used in an HVdc model. To make the new component usable for both the rectifier and inverter sides, a Boolean parameter was defined and added to the settings to distinguish between types of converters. Additionally, the feature of assigning ground to nodes of interest was included in the FS component.

(ii) Since the new component depends on steady-state equations, the dc current was used as a key parameter to be measured using a multimeter component, and to be then employed for determination of the extinction angle. Also, the extinction angle was defined as an internal output variable to be used as an input in other blocks such as the inverter alpha controller. This way, there was no need to manipulate the alpha order controllers and as minimum as changes were required to replace LCCs with the FS component.

(iii) A set of comparisons was made to ensure the efficacy of the newly developed component. The simulation results showed a runtime improvement of more than two times faster, which could be even higher in more-complicated LCC-based HVdc models.

(iv) The efficacy of the newly developed component was investigated by applying commutation failure to the ac network. The results showed that the FS component can handle commutation failure in a similar manner as the LCCs do with the help of the controllers.

5.2. Future Work

The implementation steps offer room for further testing and improvements. The possible extension of this research can be listed as follows:

(i) Although the newly developed model offers a similar overall dynamic response to what LCCs do, it still requires extra fine tuning to be able to act in place of LCCs more accurately.

(ii) The FS model can be improved to be directly used as a custom component in the library of PSCAD. To do so, there is a need to communicate with the experts in Manitoba Hydro International to follow the PSCAD/EMTDC component design requirements.

6. REFERENCES

[1] R. Wierckx, "Digital simulation of the parallel multiterminal operation of HVDC converter," University of Manitoba, Winnipeg, Manitoba, 1985.

[2] T. Gao and X. Ma, "Comparison of CCC and LCC in HVDC system," *Energy Procedia,* vol. 16, pp. 842 - 848, 2012.

[3] Manitoba HVDC Research Center, "EMTDC User's Guide," 2018.

[4] H. W. Dommel, "Digital computer solution of electromagnetic transients in single-and multiphase networks," *IEEE Transactions on Power Apparatus and Systems,* Vols. PAS-88, no. 4, pp. 388-399, 1969.

[5] A. M. Gole, S. Filizadeh, R. W. Menzies, P. L. Wilson, "Optimization-enabled electromagnetic transient simulation," *IEEE Transaction on Power Delivery,* vol. 20, no. 1, pp. 512-518, 2005.

[6] J. Arrillaga, High voltage direct current transmission, 2nd ed., vol. 29, IET Power and Energy series, 2008.

[7] "EE Power," 19 October 2020. [Online]. Available: https://eepower.com/technical-articles/the-difference-that-dc-makes/#.

[8] N. G. Hingorani, "High voltage dc transmission: a power workhorse," *IEEE Spectrum,* vol. 33, no. 4, pp. 63 - 72, 1996.

[9] D. W. Hart, Power Electronics, McGraw-Hill, 2010.

[10] H. Rissik, Mercury-arc Current Convertors, Sir Isaac Pitman and Sons Ltd., 1941.

[11] R. C. Dorf, The electrical engineering handbook (illustrated), 2nd ed., Ron Powers, 1997.

[12] W. A. Patterson, "The Eel River HVDC scheme — A 320 MW asynchronous interconnection between the New Brunswick Electric Power Commission and Hydro-Québec employing thyristor valves," *Canadian Electrical Engineering Journal,* vol. 2, no. 1, pp. 9 - 16, 1977.

[13] E. W. Kimbark, Direct Current Transmission, vol. 1, Portland, Oregon: Wiley-Interscience (a Division of John, Wiley & Sons, Inc.), 1971.

[14] Alstom (Firm), HVDC: Connecting to the Future, 2010, Alstom Grid, 2010.

[15] B. Lou, H. Zhou, Z. Xu, S. Wang and Y. Xu, "Fault Response Comparison of LCC-MMC Hybrid Topologies and Conventional HVDC Topology," *The Journal of Engineering,* vol. 2019, no. 16, pp. 2068 - 2073, 2018.

[16] M. Meisingset, "Application of capacitor commutated converters in multi-infeed HVDC schemes," The University of Manitoba, Winnipeg, Manitoba, 2000.

[17] P. Gole, "HVdc Course Notes," 2020.

[18] H. Suzuki, T. Nakajima, K. Izumi, S. Sugimoto, Y. Mino and H. Abe, "Development and testing of prototype models for a high-performance 300 MW self-commutated AC/DC converter," *IEEE Transactions on Power Delivery,* vol. 12, no. 4, pp. 1589 - 1601, October 1997.

[19] B. Qahraman, A. M. Gole and I. T. Fernando, "Hybrid HVDC converters and their impact on power system dynamic performance," in *Power Engineering Society General Meeting*, Montreal, Quebec, Canada, 2006.

[20] B. R. Anderson and L. Xu, "Hybrid HVDC system for power transmission to island networks," *IEEE Transactions on Power Delivery,* vol. 19, no. 4, pp. 1884 - 1890, October 2004.

[21] J. Lv, X. Ye, M. Yang and R. Jiao, "Research on control strategy of LCC-MMC hybrid HVDC system," in *8th Renewable Power Generation Conference (RPG 2019)*, Shanghai, 2019.

[22] S. Du, A. Dekka, B. Wu and N. Zargari, Modular Multilevel Converters: Analysis, Control, and Applications, New Jersey: John Wiley & Sons, Inc., 2017.

[23] J. Arrillaga, Y. H. Liu, N. R. Watson and N. J. Murray, Self-Commutating Converters for High Power Applications, John Wiley & Sons, Ltd, 2009.

[24] B. Qahraman and A. M. Gole, "A VSC based series hybrid converter for HVDC transmission," in *Canadian Conference on Electrical and Computer Engineering*, Saskatoon, SK, 2005.

[25] H. Xiao, Z. Xu, G. Tang and Y. Xue, "Complete mathematical model derivation for modular multilevel converter based on successive approximation approach," vol. 8, no. 12, pp. 2396 - 2410, December 2015.

[26] H. Jiang and A. Ekstrom, "Harmonic cancellation of a hybrid converter," *IEEE transaction on Power Delivery,* vol. 13, no. 4, pp. 1291 - 1296, October 1998.

[27] A. M. Gole, B. Qahraman and I. T. Fernando, "Hybrid HVDC converters and their impact on power system dynamic performance," in *IEEE Power Engineering Society General Meeting*, Montreal, QC, Canada, 2006.

[28] Z. Xu, S. Wang and H. Xiao, "Hybrid high-voltage direct current topology with line commutated converter and modular multilevel converter in series connection suitable for bulk power overhead line transmission," *IET Power Electron.,* vol. 9, no. 12, pp. 2307 - 2317, 2016.

[29] Y. Zhu, Q. Guo, C. Li, D. Chang, D. Chen and Y. Zhu, "Research on Power Modulation Strategy for MMC-HVDC and LCC-HVDC in Parallel HVDC System," in *IEEE 3rd Conference on Energy Internet and Energy System Integration (EI2)*, Changsha, China, 2019.

[30] J.-J. Jung, S. Cui, J.-H. Lee and S.-K. Sul, "A new topology of multilevel VSC converter for hybrid HVDC transmission system," *IEEE Transactions on Power Electronics,* vol. 32, no. 6, pp. 2620 -2628, August 2016.

[31] S. Dong, Y. Chi and Y. Li, "Active voltage feedback control for hybrid multi-terminal HVDC system adopting improved synchronverters," *IEEE Transactions on Power Delivery,* vol. 31, no. 2, pp. 445 - 455, April 2015.

[32] L. Xia, Y. Xiaohui, S. Xingli, F. Yunlong, L. Tao and W. Guoyang, "Research on the modeling of MMC-HVDC considering the fault ride-through characteristics," in *International Conference on Power System Technology (POWERCON)*, Guangzhou, China, 2018.

[33] M. H. Nguyen, T. K. Saha and M. Eghbal, "Master self-tuning VDCOL function for hybrid multi-terminal HVDC connecting renewable resources to a large power system," *IET Generation, Transmission & Distribution,* vol. 11, no. 13, pp. 3341 - 3349, September 2017.

[34] C. Guo, Y. Zhang, A. M. Gole and C. Zhao, "Analysis of dual-infeed HVDC with LCC–HVDC and VSC–HVDC," *IEEE Transactions on Power Delivery,* vol. 27, no. 3, pp. 1529 - 1537, July 2012.

[35] X. Li, K. Han, C. Fan, X. Li, Z. Zhang, S. Wang and Z. Xu, "Study on Main Circuit Configuration and Control Modes for a New LCC-MMC Hybrid HVDC System," in *IEEE PES Asia-Pacific Power and Energy Engineering Conference (APPEEC)*, Macao, China, 2019.

[36] H. Xiao, K. Sun, J. Pan and Y. Liu, "Operation and control of hybrid HVDC system with LCC and full-bridge MMC connected in parallel," *IET Generation, Transmission & Distribution,* vol. 14, no. 7, pp. 1344 - 1355, April 2020.

[37] J. R. Lebre and E. H. Watanabe, "Full bridge MMC control for hybrid HVDC systems," in *Brazilian Power Electronics Conference (COBEP)*, Juiz de Fora, Brazil, 2017.

[38] Aaron S. C. Leavy, Lie Xu, Shaahin Filizadeh, Aniruddha M. Gole, "Simulation-based optimization of LCC-HVDC controller parameters using surrogate model solvers," in *Workshop on Control and Modeling for Power Electronics (COMPEL)*, Toronto, ON, Canada, 2019.

[39] A. M. Gole, S. Filizadeh, R. W. Menzies, P. L. Wilson, "Electromagnetic transients simulation as an objective function evaluator for optimization of power system performance," in *International conference on power system transients - IPST*, New Orleans, USA, 2003.

[40] I, "IEEE Guide for Planning DC Links Terminating at AC Locations Having Low Short-Circuit Capacities," *IEEE Std 1204-1997,* pp. 1 - 216, 21 January 1997.

[41] Manitoba HVdc Research Centre, "PSCAD User's Guide," Winnipeg, Manitoba, Canada, 2018.

[42] M. Szechtman, T. Wess and C. V. Thio, "First benchmark model for HVDC control studies," *Electra,* vol. 135, no. 4, pp. 54 - 73, 1991.

[43] H. Yan, K. Liu, X. Wang, K. Che, Y. Ding and W. Yang, "Research on CIGRE benchmark model and improved dc control," in *Journal of Physics: Conference Series*, 2020.